

Future prospects of mass-degenerate Higgs bosons in the CP -conserving two-Higgs-doublet model

Ligong Bian^{1,2,*} Ning Chen^{3,4,†} Wei Su^{5,6,7,‡} Yongcheng Wu^{8,§} and Yu Zhang^{4,9,¶}

¹*Department of Physics, Chongqing University, Chongqing 401331, China*

²*Department of Physics, Chung-Ang University, Seoul 06974, Korea*

³*School of Physics, Nankai University, Tianjin 300071, China*

⁴*CAS Center for Excellence in Particle Physics, Beijing 100049, China*

⁵*CAS Key Laboratory of Theoretical Physics, Institute of Theoretical Physics,
Chinese Academy of Sciences, Beijing 100190, China*

⁶*School of Physics, University of Chinese Academy of Sciences, Beijing 100049, China*

⁷*Department of Physics, University of Arizona, Tucson, AZ 85721*

⁸*Ottawa-Carleton Institute for Physics, Carleton University,
1125 Colonel By Drive, Ottawa, Ontario K1S 5B6, Canada*

⁹*School of Physics, Nanjing University, Nanjing, Jiangsu, 210093, China*

(Dated: June 26, 2018)

The scenario of two mass-degenerate Higgs bosons within the general two-Higgs-doublet model (2HDM) is revisited. We focus on the global picture when two CP -even Higgs bosons of h and H are nearly mass-degenerate. A global fit to the signal strength of the 125 GeV Higgs measured at the LHC is performed. Based on the best-fit result of the 2HDM mixing angles (α, β) , theoretical constraints, charged and CP -odd Higgs boson direct search constraints and the electroweak precision constraints are imposed to the 2HDM parameter space. We present the signal predictions of the $(4b, 2b2\gamma)$ channels for the benchmark models at the LHC 14 TeV runs. We also study the direct Higgs boson pair productions at the LHC, and the Z-associated Higgs boson pair production search at the ILC 500 GeV runs, as well as the indirect probes at the CEPC 250 GeV run. We find that the mass-degenerate Higgs boson scenario in the Type-II 2HDM can be fully probed by these future experimental searches.

* lgbycl@cqu.edu.cn

† ustc0204.chenning@gmail.com

‡ weisv@itp.ac.cn

§ ycwu@physics.carleton.ca

¶ dayu@nju.edu.cn

CONTENTS

I. Introduction	2
II. The mass-degenerate Higgs bosons in the 2HDM	3
A. The global fit to the mass-degenerate Higgs boson signals at the LHC	3
B. The charged Higgs boson and EW precision constraints to the 2HDM	6
C. The perturbative unitarity and stability constraints to the 2HDM potential	9
D. The constraints from the CP -odd Higgs boson A searches	12
III. The LHC searches for degenerate Higgs bosons: constraints and pair productions	14
A. The total cross section of gluon-gluon fusion to Higgs pairs	14
B. The cross sections of Higgs pairs to various final states	16
IV. Probes of degenerate Higgs bosons at the e^+e^- colliders	17
A. The CEPC measurements of the degenerate Higgs scenario	17
B. The direct probes of the degenerate Higgs scenario at the ILC	18
V. Conclusion	21
ACKNOWLEDGMENTS	22
References	24

I. INTRODUCTION

When the 125 GeV Higgs boson was discovered at the LHC 7 \oplus 8 TeV runs [1, 2], the experimental measurements of the $\gamma\gamma$ signal rates from both ATLAS and CMS collaborations were both enhanced relative to the standard model (SM) predictions. It was suggested in Refs. [3–6] that the observed signals at ~ 125 GeV may arise from two mass-degenerate Higgs bosons.¹ Even though the obvious enhancement of the $\gamma\gamma$ rate is not shown at the LHC run-II, the scenario of two mass-degenerate Higgs bosons around 125 GeV still deserves investigation. After all, it is really challenging to distinguish this possibility from the single Higgs boson case by direct measurements of the Higgs boson mass, given that the energy resolutions of photons and leptons are typically of $\sim \mathcal{O}(1)$ GeV at the LHC [10–14]. The current mass uncertainties from the CMS measurements are ~ 0.24 GeV [15, 16]. The direct measurements of the Higgs boson(s) at 125 GeV involve their gauge couplings and Yukawa couplings at the leading order (LO). Alternatively, one may constrain such a scenario from a global point of view, by imposing various theoretical and experimental constraints.

In this work, we study the future experimental prospects of probing the mass-degenerate 125 GeV Higgs bosons at both high-luminosity (HL) LHC runs and the future high-energy colliders. Our discussions are made in the context of the CP -conserving (CPC) general 2HDM. This scenario can be constrained from the current LHC searches for the CP -odd Higgs boson A via the $h/H+Z$ decay channel. Furthermore, we suggest to distinguish the h/H mass-degenerate case from the single resonance case through the probes of the Higgs boson self couplings. This can be done by searching for the Higgs boson pair production processes at both LHC and the future high-energy colliders. For the new physics (NP) models involving a single 125 GeV Higgs boson, it is quite often that the modified Higgs cubic self couplings (including the additional resonances) are the only sources to modify the Higgs pair production cross sections. The signal rates for various final states can be estimated by using the SM-like Higgs boson decay branching fractions (see Ref. [17] for the summary). There have been extensive discussions of the Higgs boson pair productions in various beyond standard model (BSM) NP models [18–23]. Currently, two most sensitive search modes for the Higgs boson pair productions at the LHC 13 TeV run are $(4b, 2b2\gamma)$ [24–29]. For the Higgs pair productions with two mass-degenerate Higgs bosons, one may expect: (i) the deviation of Higgs cubic self-couplings from the SM predictions, and (ii) the existence of multiple Higgs cubic self-couplings, hence, multiple processes contributing to each final state.

The layout of this paper is described as follows. In Sec. II, we review the scenario of degenerate Higgs bosons in the framework of CPC 2HDM. The LHC measurements of the Higgs signal strengths are used for the global fit, where we simplify the discussion with negligible quantum interference and mixing effects. This can be achieved by assuming sufficiently large mass splitting. Other constraints, such as the perturbative unitarity and stability of the 2HDM potential, the EW precision tests, as

¹ The previous estimations of the signal rates were performed by summing up the cross sections times decay branching fractions of individual Higgs boson [3, 4, 7]. Recently, it was pointed out in Ref. [8] that the quantum interference effect should be taken into account for the signal rates from two CP -even Higgs bosons (see also Ref. [9] for the NMSSM case). This effect was found to be significant when the mass splitting are comparable or smaller than the total decay widths of two nearly degenerate Higgs bosons.

well as the LHC direct searches for the CP -odd Higgs boson A , are also considered for the 2HDM with mass-degenerate h/H . The benchmark points are suggested for both Type-I and Type-II 2HDM. In Sec. III, we study the gluon-gluon fusion (ggF) productions of Higgs pairs at the LHC for the degenerate Higgs scenario. We compare the signal predictions from various final states of $(4b, 2b2\gamma)$ with the corresponding SM predictions at the LO. Their cross sections are generally varying with different soft mass terms of m_{12} in the 2HDM potential. In particular, we find that the signal rates of $(4b, 2b2\gamma)$ final states are always moderately enhanced with respect to the SM predictions. The corresponding significances are estimated for the h/H mass-degenerate case as well. In Sec. IV, we discuss the capability of distinguishing the h/H mass-degenerate scenario at the future high-energy e^+e^- colliders. We show the indication from the precise measurement of cross sections of mass-degenerate Higgs bosons with Z -boson for this scenario at the circular electron-positron collider (CEPC). Furthermore, the direct production of Higgs boson pairs associated with Z -boson at the ILC can probe the h/H mass-degenerate scenario in the Type-II 2HDM. The summaries are given in Sec. V.

II. THE MASS-DEGENERATE HIGGS BOSONS IN THE 2HDM

A. The global fit to the mass-degenerate Higgs boson signals at the LHC

In the CPC 2HDM, there are five Higgs bosons of (h, H, A, H^\pm) in the scalar mass spectrum. The review of the 2HDM setup and the related LHC phenomenology can be found in Refs. [7, 30]. The Lagrangian for the general 2HDM is written as follows

$$\mathcal{L} = \mathcal{L}_{\text{kin}} + \mathcal{L}_{\text{Yukawa}} - V(\Phi_1, \Phi_2), \quad (1a)$$

$$\mathcal{L}_{\text{kin}} = |D_\mu \Phi_1|^2 + |D_\mu \Phi_2|^2, \quad (1b)$$

$$\begin{aligned} V(\Phi_1, \Phi_2) = & m_{11}^2 |\Phi_1|^2 + m_{22}^2 |\Phi_2|^2 - m_{12}^2 (\Phi_1^\dagger \Phi_2 + H.c.) \\ & + \frac{1}{2} \lambda_1 (\Phi_1^\dagger \Phi_1)^2 + \frac{1}{2} \lambda_2 (\Phi_2^\dagger \Phi_2)^2 + \lambda_3 |\Phi_1|^2 |\Phi_2|^2 + \lambda_4 |\Phi_1^\dagger \Phi_2|^2 \\ & + \frac{1}{2} \lambda_5 [(\Phi_1^\dagger \Phi_2)^2 + H.c.]. \end{aligned} \quad (1c)$$

All parameters are assumed to be real for the CPC case. Very often, a softly broken \mathbb{Z}_2 symmetry, under which two Higgs doublets transform as $(\Phi_1, \Phi_2) \rightarrow (\Phi_1, -\Phi_2)$, is also assumed to eliminate the possible $\lambda_{6,7}$ couplings in the 2HDM potential. One has $m_{12} = 0$ when the \mathbb{Z}_2 symmetry is exact. Two Higgs doublets of $\Phi_{1,2}$ can be expressed in terms of components as

$$\Phi_1 = \begin{pmatrix} \pi_1^+ \\ \frac{1}{\sqrt{2}}(v_1 + h_1 + i\pi_1^0) \end{pmatrix}, \quad \Phi_2 = \begin{pmatrix} \pi_2^+ \\ \frac{1}{\sqrt{2}}(v_2 + h_2 + i\pi_2^0) \end{pmatrix}, \quad (2)$$

with two Higgs vacuum expectation values (VEVs) and their ratios being

$$v_1^2 + v_2^2 = (\sqrt{2}G_F)^{-1} \simeq (246 \text{ GeV})^2, \quad t_\beta \equiv v_2/v_1. \quad (3)$$

Here, $\pi_{1,2}^0$ are pseudoreal components, whose linear combinations of $A = -s_\beta\pi_1^0 + c_\beta\pi_2^0$ and $G = c_\beta\pi_1^0 + s_\beta\pi_2^0$ are CP -odd Higgs boson and neutral Nambu-Goldstone boson, respectively. $\pi_{1,2}^\pm$ (and their complex conjugates) are complex scalar fields, whose linear combinations of $H^\pm = -s_\beta\pi_1^\pm + c_\beta\pi_2^\pm$ and $G^\pm = c_\beta\pi_1^\pm + s_\beta\pi_2^\pm$ are charged Higgs bosons and charged Nambu-Goldstone bosons, respectively.

For further discussion, we list the dimensionless Higgs gauge couplings and Yukawa couplings as follows

$$\mathcal{L} \supset \sum_{h_i=h,H} \left[-\frac{m_f}{v} \xi_i^f \bar{f} f + a_i \left(2\frac{m_W^2}{v} W_\mu^+ W^{-\mu} + \frac{m_Z^2}{v} Z_\mu Z^\mu \right) \right] h_i - \frac{m_f}{v} \xi_A^f \bar{f} i \gamma_5 f A, \quad (4)$$

with

$$\begin{aligned} \text{Type-I: } \xi_h^f &= s_{\beta-\alpha} + \frac{c_{\beta-\alpha}}{t_\beta}, & \xi_H^f &= c_{\beta-\alpha} - \frac{s_{\beta-\alpha}}{t_\beta} \\ \xi_A^u &= \frac{1}{t_\beta}, & \xi_A^{d,\ell} &= -\frac{1}{t_\beta}, \end{aligned} \quad (5a)$$

$$\begin{aligned} \text{Type-II: } \xi_h^u &= s_{\beta-\alpha} + \frac{c_{\beta-\alpha}}{t_\beta}, & \xi_h^{d,\ell} &= s_{\beta-\alpha} - c_{\beta-\alpha} t_\beta, \\ \xi_H^u &= c_{\beta-\alpha} - \frac{s_{\beta-\alpha}}{t_\beta}, & \xi_H^{d,\ell} &= c_{\beta-\alpha} + s_{\beta-\alpha} t_\beta, \\ \xi_A^u &= \frac{1}{t_\beta}, & \xi_A^{d,\ell} &= t_\beta, \end{aligned} \quad (5b)$$

$$a_h = s_{\beta-\alpha}, \quad a_H = c_{\beta-\alpha}. \quad (5c)$$

Here, α represents the mixing angle between two CP -even Higgs bosons of (h, H) .

The overall signal rates are controlled by the input parameters of (α, β) in the CPC 2HDM, which is manifest from the couplings in Eqs. (5). A global fit to the h/H degenerate scenario respect to (α, β) is thus performed, and this is done by the χ^2 fit to the LHC data defined as

$$\chi^2 = \sum_{\text{PD}} \left(\frac{\mu_{\text{th}}^{\text{PD}} - \mu_{\text{exp}}^{\text{PD}}}{\sigma_{\text{exp}}^{\text{PD}}} \right)^2, \quad (6)$$

where the current LHC measurements of signal strengths and errors of $(\mu_{\text{exp}}^{\text{PD}}, \sigma_{\text{exp}}^{\text{PD}})$ are summarized in Tables I and II for the run-I and run-II data, respectively.

This scenario was previously explored in Refs. [3–7], where the total signal rates for 125 GeV Higgs boson were estimated by simple summation of $\sigma \times \text{Br}$ from the individual contribution of h and H as

$$\mu[XX \rightarrow h/H \rightarrow YY] = \frac{|\kappa_{hXX} \kappa_{hYY}|^2}{\Gamma_h / \Gamma_h^{\text{SM}}} + \frac{|\kappa_{HXX} \kappa_{HYY}|^2}{\Gamma_H / \Gamma_h^{\text{SM}}}. \quad (7)$$

This is valid when the mass splitting between two resonances of h and H are sufficiently large such that the quantum interference between two amplitudes are negligible. Quantitatively, the sufficiently large mass splitting refers to the case when $\Delta M \equiv M_H - M_h \gg \Gamma_H + \Gamma_h$ [8]. To

Decays	Productions	ATLAS	Ref	CMS	Ref
$\gamma\gamma$	ggF	1.32 ± 0.38	[31]	$1.12_{-0.32}^{+0.37}$	[32]
$\gamma\gamma$	VBF	0.8 ± 0.7	[31]	$1.58_{-0.68}^{+0.77}$	[32]
$\gamma\gamma$	WH	1.0 ± 1.6	[31]
$\gamma\gamma$	ZH	$0.1_{-0.1}^{+3.7}$	[31]
$\gamma\gamma$	VH	$-0.16_{-0.79}^{+1.16}$	[32]
$\gamma\gamma$	ttH	$1.6_{-1.8}^{+2.7}$	[31]	$2.69_{-1.81}^{+2.51}$	[32]
ZZ	ggF,ttH,bbH	$1.7_{-0.4}^{+0.5}$	[33]
ZZ	ggF,ttH	$0.80_{-0.36}^{+0.46}$	[34]
ZZ	VBF,VH	$0.3_{-0.9}^{+1.6}$	[33]	$1.7_{-2.1}^{+2.2}$	[34]
W^+W^-	ggF	$1.02_{-0.26}^{+0.29}$	[35]	$0.74_{-0.20}^{+0.22}$	[36]
W^+W^-	VBF	$1.27_{-0.45}^{+0.53}$	[35]	$0.60_{-0.46}^{+0.57}$	[36]
W^+W^-	VH	$0.39_{-1.87}^{+1.97}$	[36]
$b\bar{b}$	ttH	1.5 ± 1.1	[37]	$1.2_{-1.5}^{+1.6}$	[38]
$b\bar{b}$	VH	$0.51_{-0.37}^{+0.40}$	[39]	1.0 ± 0.5	[40]
$\tau^+\tau^-$	ggF	$2.0_{-1.2}^{+1.5}$	[41]	1.07 ± 0.46	[42]
$\tau^+\tau^-$	VBF,VH	$1.24_{-0.54}^{+0.59}$	[41]
$\tau^+\tau^-$	VBF	0.94 ± 0.41	[42]
$\tau^+\tau^-$	VH	-0.33 ± 1.02	[42]

TABLE I. Signal strengths of Higgs searches measured by the ATLAS and CMS collaborations, for various decay and production channels for the $\sqrt{s} = 7 \oplus 8$ TeV runs.

simplify our discussions, we still use the simple summation method in Eq. (7) to estimate the total signal rates for various channels. The global fit results on the (α, β) plane are shown in Fig. 1. The corresponding benchmark points for the mass-degenerate $M_h \approx M_H = 125$ GeV cases are listed in Table. III for both Type-I and Type-II 2HDM. We also observe that a shift of $\alpha \rightarrow \alpha - \pi/2$ leads to equally minimal χ^2 values in both Type-I and Type-II cases. This corresponds to an interchange between h and H in the mass-degenerate scenario. Besides the 2HDM parameters of (α, β) , the total decay widths of $\Gamma_h + \Gamma_H$ and the main decay branching fractions are also listed for the mass-degenerate case. Since the total decay widths of $\Gamma_h + \Gamma_H$ are smaller than $\sim \mathcal{O}(0.1)$ GeV, our simplification in Eq. (7) is valid. The alignment parameters are $c_{\beta-\alpha} = 0.21$ for the Type-I 2HDM and $c_{\beta-\alpha} = 0.01$ for the Type-II 2HDM, respectively. A sizable deviation from the alignment limit is observed in the Type-I benchmark point. For the Type-II case, meanwhile, the H is gauge-phobic and decays mostly into fermionic final states of $(b\bar{b}, \tau^+\tau^-)$. Throughout the context below, we shall always use the best-fit points of (α, β) in Table. III for the phenomenology discussions in

Decays	Productions	ATLAS	Ref	CMS	Ref
$\gamma\gamma$	ggF	$0.80^{+0.19}_{-0.18}$	[43, 44]	$1.11^{+0.19}_{-0.18}$	[45]
$\gamma\gamma$	VBF	2.1 ± 0.6	[43, 44]	$0.5^{+0.6}_{-0.5}$	[45]
$\gamma\gamma$	VH	$0.7^{+0.9}_{-0.8}$	[43, 44]	$2.3^{+1.1}_{-1.0}$	[45]
$\gamma\gamma$	ttH	0.5 ± 0.6	[43, 44]	$2.2^{+0.9}_{-0.8}$	[45]
ZZ	ggF	$1.11^{+0.25}_{-0.22}$	[44, 46]	$1.20^{+0.22}_{-0.21}$	[47]
ZZ	VBF	$4.0^{+1.8}_{-1.5}$	[44, 46]	$0.05^{+1.03}_{-0.05}$	[47]
ZZ	VH	0 ± 1.9	[44, 46]	0 ± 2.83 , or 0 ± 2.66	[47]
ZZ	ttH	0 ± 3.9	[44, 46]	0 ± 1.19	[47]
W^+W^-	ggF	1.02 ± 0.27	[48]
W^+W^-	VBF	$1.7^{+1.2}_{-0.9}$	[49]
W^+W^-	WH	$3.2^{+4.4}_{-4.2}$	[49]
W^+W^-	VBF+VH	0.89 ± 0.67	[48]
$b\bar{b}$	VH	$1.20^{+0.42}_{-0.36}$	[50]
$\tau^+\tau^-$	ggF	0.84 ± 0.89	[51]
$\tau^+\tau^-$	VBF	$1.11^{+0.34}_{-0.35}$	[51]
$\tau^+\tau^-$	ttH	$0.72^{+0.62}_{-0.53}$	[52]

TABLE II. Signal strengths of Higgs searches measured by the ATLAS and CMS collaborations, for various decay and production channels for the $\sqrt{s} = 13$ TeV runs.

the mass-degenerate scenario.

Besides the best-fit points from the current LHC Higgs data, we shall further impose theoretical and experimental constraints to the 2HDM mass spectrum of (M_A, M_{\pm}, m_{12}) in the following context, for the mass-degenerate Higgs boson scenario. We shall show that mass-degenerate Higgs boson scenario has allowed 2HDM parameter space with all these constraints imposed.

B. The charged Higgs boson and EW precision constraints to the 2HDM

It is known that the charged Higgs bosons of H^{\pm} contribute to the flavor-changing neutral current (FCNC) rare decay processes, such as $b \rightarrow s\gamma$ transition. The latest measurement is from the Belle Collaboration [53], and the implication to the CPC 2HDM was carried out in Refs. [54–57]. By imposing the FCNC constraints to the benchmark models in Table. III, we get $M_{\pm} \gtrsim 590$ GeV in the Type-II 2HDM, while the lower mass bound in the Type-I 2HDM is negligible, as compared to the direct collider constraints. Besides, the direct searches for the charged Higgs bosons at the LHC were performed in Refs. [58–60]. Here, we shall only consider the FCNC constraints to the

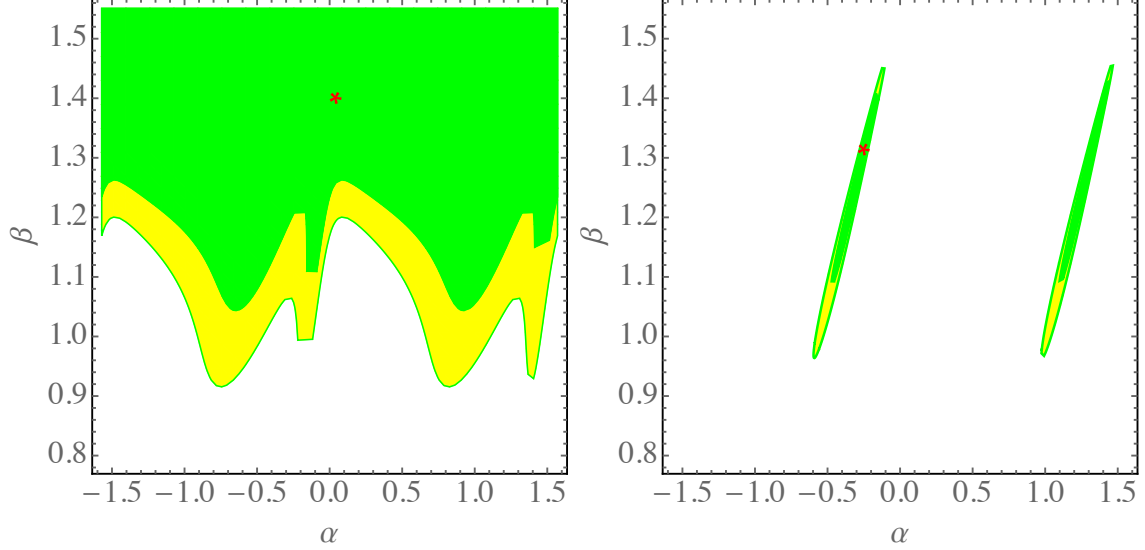


FIG. 1. The global fit of two mass-degenerate Higgs bosons in the Type-I (left panel) and Type-II (right panel) 2HDM on the (α, β) plane. The yellow and green regions are the $(1, 2)\sigma$ allowed regions of the LHC $7 \oplus 8 \oplus 13$ TeV Higgs data fitting, and the benchmark points are marked by red stars.

$M_h \approx M_H$	Type-I	Type-II
$(\alpha, \beta, \Gamma_{\text{tot}})$	(0.04263, 1.3995, 4.16 MeV)	(-0.2495, 1.3121, 41.38 MeV)
(Γ_h, Γ_H)	(4.11 MeV, 0.05 MeV)	(3.89 MeV, 37.49 MeV)
$(\text{Br}[h \rightarrow b\bar{b}], \text{Br}[H \rightarrow b\bar{b}])$	(58.80%, 8.68%)	(56.23%, 89.85%)
$(\text{Br}[h \rightarrow \tau^+\tau^-], \text{Br}[H \rightarrow \tau^+\tau^-])$	(6.44%, 0.95%)	(6.16%, 9.84%)
$(\text{Br}[h \rightarrow W^+W^-], \text{Br}[H \rightarrow W^+W^-])$	(20.35%, 77.86%)	(22.50%, -)
$(\text{Br}[h \rightarrow ZZ], \text{Br}[H \rightarrow ZZ])$	(2.50%, 9.56%)	(2.76%, -)
$(\text{Br}[h \rightarrow \gamma\gamma], \text{Br}[H \rightarrow \gamma\gamma])$	(0.21%, 1.22%)	(0.24%, -)
$(\text{Br}[h \rightarrow gg], \text{Br}[H \rightarrow gg])$	(8.73%, 1.29%)	(9.04%, 0.28%)

TABLE III. The best-fit points of (α, β) for the mass-degenerate Higgs bosons of $M_h \approx M_H = 125$ GeV in both Type-I and Type-II 2HDM. The decay widths of (Γ_h, Γ_H) , and decay branching ratios are listed, where the decay branching ratios smaller than 10^{-4} are neglected.

charged Higgs boson mass, and leave the direct LHC search limits to the charged Higgs bosons in the context of the mass-degenerate Higgs bosons. This is valid because: (i) the FCNC constraints are only relevant to the charged Higgs Yukawa couplings, and (ii) the decay modes of the charged Higgs bosons can be significantly modified in the mass-degenerate Higgs boson scenario. To simplify, we

shall take $M_{\pm} = M_A$ for the Type-I 2HDM ², and fix $M_{\pm} = 600$ GeV for the Type-II 2HDM below ³.

We consider the constraints from the EW precision tests [61–63] to the 2HDM with mass-degenerate h/H . The most general expressions for $(\Delta S, \Delta T)$ in the CPC 2HDM [61] read

$$\begin{aligned} \Delta S = & \frac{1}{\pi m_Z^2} \left\{ \left[\mathcal{B}_{22}(m_Z^2; M_H^2, M_A^2) - \mathcal{B}_{22}(m_Z^2; M_{\pm}^2, M_{\pm}^2) \right] \right. \\ & + \left[\mathcal{B}_{22}(m_Z^2; M_h^2, M_A^2) - \mathcal{B}_{22}(m_Z^2; M_H^2, M_A^2) + \mathcal{B}_{22}(m_Z^2; m_Z^2, M_H^2) - \mathcal{B}_{22}(m_Z^2; m_Z^2, M_h^2) \right. \\ & \left. \left. - m_Z^2 \mathcal{B}_0(m_Z; m_Z, M_H^2) + m_Z^2 \mathcal{B}_0(m_Z; m_Z, M_h^2) \right] c_{\beta-\alpha}^2 \right\}, \end{aligned} \quad (8a)$$

$$\begin{aligned} \Delta T = & \frac{1}{16\pi m_W^2 s_W^2} \left\{ \left[F(M_{\pm}^2, M_A^2) + F(M_{\pm}^2, M_H^2) - F(M_A^2, M_H^2) \right] \right. \\ & + \left[F(M_{\pm}^2, M_h^2) - F(M_{\pm}^2, M_H^2) - F(M_A^2, M_h^2) + F(M_A^2, M_H^2) \right. \\ & + F(m_W^2, M_H^2) - F(m_W^2, M_h^2) - F(m_Z^2, M_H^2) + F(m_Z^2, M_h^2) \\ & \left. \left. + 4m_Z^2 \bar{\mathcal{B}}_0(m_Z^2, M_H^2, M_h^2) - 4m_W^2 \bar{\mathcal{B}}_0(m_W^2, M_H^2, M_h^2) \right] c_{\beta-\alpha}^2 \right\}, \end{aligned} \quad (8b)$$

where we explicitly split these expressions into terms independent of or dependent on the alignment parameter of $c_{\beta-\alpha}$. The relevant auxiliary functions read

$$F(x_1, x_2) \equiv \begin{cases} \frac{x_1+x_2}{2} - \frac{x_1 x_2}{x_1-x_2} \ln \frac{x_1}{x_2} & x_1 \neq x_2 \\ 0 & x_1 = x_2 \end{cases} \quad (9a)$$

$$f(x_1, x_2) \equiv \begin{cases} -2\sqrt{\Delta} \left[\tan^{-1} \frac{x_1-x_2+1}{\sqrt{\Delta}} - \tan^{-1} \frac{x_1-x_2-1}{\sqrt{\Delta}} \right] & \Delta > 0 \\ 0 & \Delta = 0 \\ \sqrt{-\Delta} \ln \frac{x_1+x_2-1+\sqrt{-\Delta}}{x_1+x_2-1-\sqrt{-\Delta}} & \Delta < 0 \end{cases} \quad (9b)$$

$$\Delta = 2(x_1 + x_2) - (x_1 - x_2)^2 - 1, \quad (9c)$$

$$\mathcal{B}_0(q^2; m_1^2, m_2^2) \equiv 1 + \frac{1}{2} \left[\frac{x_1 + x_2}{x_1 - x_2} - (x_1 - x_2) \right] \ln \frac{x_1}{x_2} + \frac{1}{2} f(x_1, x_2), \quad (9d)$$

$$\begin{aligned} \mathcal{B}_{22}(q^2; m_1^2, m_2^2) \equiv & \frac{q^2}{24} \left\{ 2 \ln q^2 + \ln(x_1 x_2) + \left[(x_1 - x_2)^3 - 3(x_1^2 - x_2^2) + 3(x_1 - x_2) \right] \ln \frac{x_1}{x_2} \right. \\ & - \left[2(x_1 - x_2)^2 - 8(x_1 + x_2) + \frac{10}{3} \right] \\ & \left. - \left[(x_1 - x_2)^2 - 2(x_1 + x_2) + 1 \right] f(x_1, x_2) - 6F(x_1, x_2) \right\}, \end{aligned} \quad (9e)$$

$$\bar{\mathcal{B}}_0(m_1^2, m_2^2, m_3^2) \equiv \frac{m_1^2 \ln m_1^2 - m_3^2 \ln m_3^2}{m_1^2 - m_3^2} - \frac{m_1^2 \ln m_1^2 - m_2^2 \ln m_2^2}{m_1^2 - m_2^2}, \quad (9f)$$

with $x_i = m_i^2/q^2$. The current Gfitter fit [64] to the EW data gives

$$S = 0.05 \pm 0.11, \quad T = 0.09 \pm 0.13. \quad (10)$$

² As we shall see below, the specific mass ranges of (M_{\pm}, M_A) do not play a role in the Higgs boson pair productions at the LHC or ILC. Without loss of generality, we make such simplification of $M_{\pm} = M_A$.

³ When taking the unitarity bound into account, it turns out that the charged Higgs boson mass cannot exceed ~ 625 GeV. Thus, a fixed $M_{\pm} = 600$ GeV is taken to compromise the joint constraints from the FCNC rare decay and unitarity for the Type-II case.

For benchmark models in both Type-I and Type-II cases, the alignment parameters were found to be small as from Table. III. Thus, the 2HDM contributions to the $(\Delta S, \Delta T)$ are mainly controlled by leading terms in the first lines of Eqs. (8). By using the definitions of auxiliary functions of (9a) and (9e), the $(\Delta S, \Delta T)$ can be suppressed with degenerate mass inputs of $M_A = M_\pm$. Indeed, by using the best-fit (α, β) inputs for the h/H degenerate cases in Table. III, we find $(\Delta S, \Delta T) \sim (-10^{-4}, -10^{-7})$ with $M_A = M_\pm$ for the Type-I 2HDM, and $(\Delta S, \Delta T) \sim (-10^{-4}, 10^{-2})$ with $M_A \in (200, 300)$ GeV and fixed $M_\pm = 600$ GeV input for the Type-II 2HDM ⁴.

C. The perturbative unitarity and stability constraints to the 2HDM potential

The joint constraints of the perturbative unitarity and tree-level stability conditions to the 2HDM potential turns out to be powerful to bound the heavy scalar masses. The conditions to be satisfied for the unitarity constraints to the 2HDM potential are that the absolute values of the following linear combinations of the quartic scalar couplings [65, 66]:

$$\begin{aligned}
a_\pm &= \frac{3}{2}(\lambda_1 + \lambda_2) \pm \frac{1}{2}\sqrt{9(\lambda_1 - \lambda_2)^2 + (2\lambda_3 + \lambda_4)^2}, \\
b_\pm &= \frac{1}{2}\left[(\lambda_1 + \lambda_2) \pm \sqrt{(\lambda_1 - \lambda_2)^2 + 4\lambda_4^2}\right], \\
c_\pm &= \frac{1}{2}\left[(\lambda_1 + \lambda_2) \pm \sqrt{(\lambda_1 - \lambda_2)^2 + 4\lambda_5^2}\right], \\
f_+ &= \lambda_3 + 2\lambda_4 + 3\lambda_5, & f_- &= \lambda_3 + \lambda_5, & f_1 &= f_2 = \lambda_3 + \lambda_4, \\
e_1 &= \lambda_3 + 2\lambda_4 - 3\lambda_4, & e_2 &= 2\lambda_3 - \lambda_5, & p_1 &= \lambda_3 - \lambda_4,
\end{aligned} \tag{11}$$

should be smaller than or equal to 8π . The tree-level vacuum stability conditions for the general 2HDM potential come from the requirement that the scalar potential being bounds from below, which read [67] ⁵

$$\lambda_{1,2} \geq 0, \quad \lambda_3 \geq -\sqrt{\lambda_1 \lambda_2}, \quad \lambda_3 + \lambda_4 - |\lambda_5| \geq -\sqrt{\lambda_1 \lambda_2}. \tag{12}$$

The quartic self couplings of λ_i are related to the Higgs boson masses, the mixing angles, and the soft mass term as follows

$$\lambda_1 = \frac{M_h^2 s_\alpha^2 + M_H^2 c_\alpha^2 - m_{12}^2 t_\beta}{v^2 c_\beta^2}, \tag{13a}$$

$$\lambda_2 = \frac{M_h^2 c_\alpha^2 + M_H^2 s_\alpha^2 - m_{12}^2/t_\beta}{v^2 s_\beta^2}, \tag{13b}$$

$$\lambda_3 = \frac{1}{v^2} \left[\frac{(M_H^2 - M_h^2) s_\alpha c_\alpha}{s_\beta c_\beta} + 2M_\pm^2 - \frac{m_{12}^2}{s_\beta c_\beta} \right], \tag{13c}$$

$$\lambda_4 = \frac{1}{v^2} (M_A^2 - 2M_\pm^2 + \frac{m_{12}^2}{s_\beta c_\beta}), \tag{13d}$$

⁴ Here, we take the mass range of $M_A \in (200, 300)$ GeV by considering the perturbative unitarity constraint and the direct search limit of $A \rightarrow hZ$ at the LHC.

⁵ Recently, it was suggested in Ref. [68] to apply the global minimum condition to constrain the 2HDM potential. In Ref. [69], the loop effects to the vacuum stability conditions were found to alleviate the tree-level conditions.

$$\lambda_5 = \frac{1}{v^2} \left(\frac{m_{12}^2}{s_\beta c_\beta} - M_A^2 \right). \quad (13e)$$

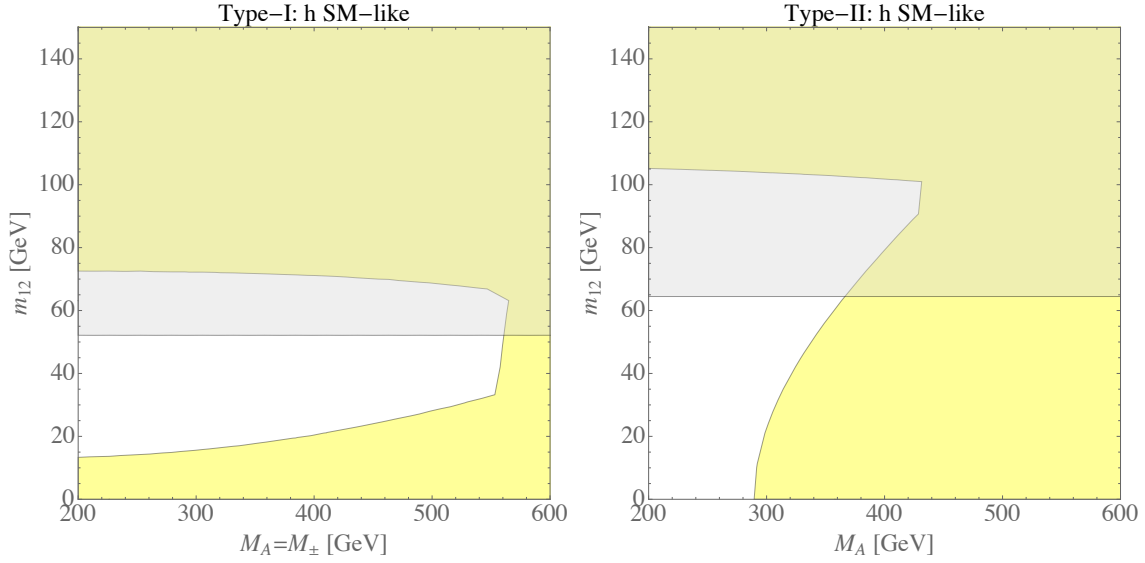


FIG. 2. The unitarity (yellow) and stability (gray) excluded regions for Type-I (left) and Type-II (right) 2HDM, with the $M_h \approx M_H = 125$ GeV scenario. The best-fit points of $(\alpha, \beta) = (0.04, 1.40)$ for Type-I case and $(\alpha, \beta) = (-0.25, 1.31)$ for Type-II case are taken as in Table. III. On the right panel, we fix $M_\pm = 600$ GeV to evade the B-physics constraints in the Type-II case.

By combining the constraints in Eq. (11) and Eq. (12) and using the quartic self couplings given in Eqs. (13), we show the joint unitarity and stability constraints in Fig. 2 for Type-I and Type-II 2HDM. The best-fit points of (α, β) for Type-I and Type-II cases are used as in Table. III. As mentioned in the previous subsection, a fixed charged Higgs boson mass of $M_\pm = 600$ GeV is always taken in the Type-II case to evade the B-physics constraints. For the best-fit points of (α, β) in Table. III, a larger m_{12} leads to a larger negative scalar quartic couplings λ_1 as indicated by Eq. (13a), therefore results in the perturbative unitarity (mostly from the $|a_-| \leq 8\pi$) and stability bounds on the m_{12} , as depicted by the two panels of Fig. 2. For the fixed m_{12} , one can expect a larger positive λ_3 for larger heavy Higgs boson masses. This breaks the perturbative unitarity through quartic coupling combination of e_2 , therefore sets the upper bounds on the heavy Higgs boson masses for both Type-I and Type-II 2HDM. For the fixed heavy Higgs boson masses of $M_A = M_\pm$ in the Type-I case, a smaller m_{12} leads to a relatively larger positive λ_1 . This results in a larger $|a_+|$, which in turn gives the lower bounds on m_{12} on the left panel of Fig. 2. The upper bounds to the mass mixing of m_{12} in the Higgs potential set by the unitarity constraints and the stability constraints, which mainly come from the fact that the mass of the second CP -even Higgs boson M_H is fixed. Correspondingly, the quartic scalar couplings of $\lambda_{1,2}$ are determined by m_{12} for the best-fit points. Since the m_{12} enters into the Higgs cubic self couplings, we take their ranges to be

$$\text{Type-I: } 20 \lesssim m_{12} \lesssim 50 \text{ GeV, with } M_A = M_\pm \in (200, 280) \text{ GeV,}$$

Type-II : $0 \leq m_{12} \lesssim 60$ GeV ,

$$\text{with } M_A \in (200, 250) \text{ GeV and } M_{\pm} = 600 \text{ GeV.} \quad (14)$$

Here, we also limit the heavy Higgs boson masses of (M_A, M_{\pm}) in the ranges that are consistent with the current LHC run-II searches for the CP -odd Higgs boson A in the mass-degenerate scenario, as indicated in Fig. 4 below.

The coefficients of the Higgs cubic self couplings in the physical basis will be used in the calculation of the direct Higgs pair productions at the LHC and the ILC, which are listed as follows

$$\lambda_{hhh} = -\frac{1}{32vs_{\beta}^2c_{\beta}^2} \left[M_h^2(3s_{\alpha-\beta} + s_{3(\alpha-\beta)} - s_{3\alpha+\beta} - 3s_{\alpha+3\beta}) + 4m_{12}^2(c_{3\alpha-\beta} + c_{\alpha-3\beta} + 2c_{\alpha+\beta}) \right], \quad (15a)$$

$$\lambda_{hhH} = \frac{c_{\alpha-\beta}}{2vs_{\beta}c_{\beta}} \left[(2M_h^2 + M_H^2)s_{\alpha}c_{\alpha} + m_{12}^2(1 - 3\frac{s_{2\alpha}}{s_{2\beta}}) \right], \quad (15b)$$

$$\lambda_{hHH} = \frac{s_{\beta-\alpha}}{2vs_{\beta}c_{\beta}} \left[-(M_h^2 + 2M_H^2)s_{\alpha}c_{\alpha} + m_{12}^2(1 + 3\frac{s_{2\alpha}}{s_{2\beta}}) \right], \quad (15c)$$

$$\lambda_{HHH} = -\frac{1}{32vs_{\beta}^2c_{\beta}^2} \left[M_H^2(c_{3(\alpha-\beta)} - c_{3\alpha+\beta} - 3c_{\alpha-\beta} + 3c_{\alpha+3\beta}) + 4m_{12}^2(s_{\alpha-3\beta} - s_{3\alpha-\beta} + 2s_{\alpha+\beta}) \right]. \quad (15d)$$

In the alignment limit of $\beta - \alpha = \pi/2$, they become

$$\lambda_{hhh} \rightarrow \frac{M_h^2}{2v}, \quad (16a)$$

$$\lambda_{hhH} \rightarrow 0, \quad (16b)$$

$$\lambda_{hHH} \rightarrow \frac{1}{2v} \left(M_h^2 + 2M_H^2 - 2\frac{m_{12}^2}{s_{\beta}c_{\beta}} \right), \quad (16c)$$

$$\lambda_{HHH} \rightarrow -\frac{1}{vt_{2\beta}} \left(M_H^2 - \frac{m_{12}^2}{s_{\beta}c_{\beta}} \right). \quad (16d)$$

In Fig. 3, we display the Higgs cubic self couplings versus the soft mass term m_{12} , with the unitarity/stability constraints in Eq. (14) taken into account for two best-fit points listed in Table. III. It turns out that the Higgs cubic self couplings of λ_{hhh} are very close to the SM value of $\lambda_{hhh}^{\text{SM}} \simeq 32$ GeV in both Type-I and Type-II 2HDM. The Higgs cubic self couplings of λ_{hhH} are suppressed by the alignment parameter of $c_{\beta-\alpha}$. With $c_{\beta-\alpha} = 0.21$ in Type-I and $c_{\beta-\alpha} = 0.01$ in Type-II 2HDM, λ_{hhH} approaches to zero for the allowed range of m_{12} . Jointly, one can envision that the cross sections of $\sigma[e^+e^- \rightarrow hhZ]$ at the ILC 500 GeV run are almost independent of the m_{12} inputs. The Higgs cubic self couplings of λ_{hHH} increase from -15 GeV to 28 GeV, with $m_{12} \in (20, 50)$ GeV in the Type-I case; or decrease from 92 GeV to 36 GeV, with $m_{12} \in (0, 60)$ GeV in the Type-II case. Such behaviors are relevant to the relation between the $\sigma[e^+e^- \rightarrow HHZ]$ at the ILC 500 GeV run and the m_{12} inputs. The Higgs cubic self couplings of λ_{HHH} are always positive in both Type-I and Type-II cases.

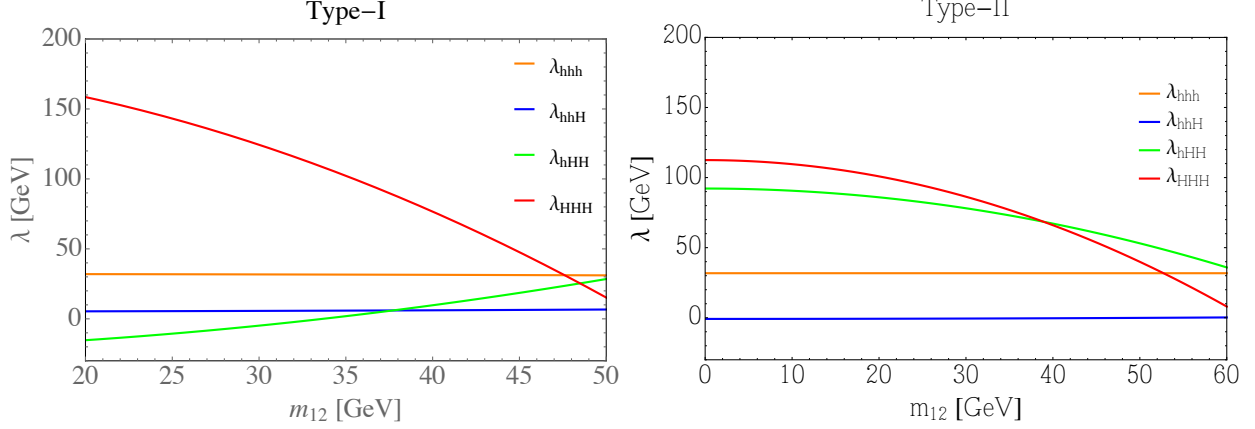


FIG. 3. The dependences of the relevant Higgs cubic self couplings λ_{hhh} (orange), λ_{hhH} (blue), λ_{hHH} (green), and λ_{HHH} (red) on the soft mass term m_{12} in the Type-I (left) and Type-II (right) 2HDM. The best-fit points of $(\alpha, \beta) = (0.04, 1.40)$ for Type-I case and $(\alpha, \beta) = (-0.25, 1.31)$ for Type-II case are taken as in Table. III. The ranges of m_{12} are taken as in Eq. (14) for Type-I and Type-II cases.

D. The constraints from the CP -odd Higgs boson A searches

Before we discuss the degenerate Higgs boson pair searches at the LHC, we impose the constraints via the LHC searches for the CP -odd Higgs boson A in the mass-degenerate h/H scenario. The decay modes and the corresponding partial decay widths of CP -odd Higgs boson A are

$$\Gamma[A \rightarrow gg] = \frac{G_F \alpha_s^2 M_A^3}{64\sqrt{2}\pi^3} \left| \sum_q \xi_A^q A_{1/2}^A(\tau_q) \right|^2, \quad (17a)$$

$$\Gamma[A \rightarrow f\bar{f}] = \frac{G_F m_f^2 M_A}{4\sqrt{2}\pi} N_{c,f} (\xi_A^f)^2 \sqrt{1 - \frac{4m_f^2}{M_A^2}}, \quad (17b)$$

$$\begin{aligned} \Gamma[A \rightarrow hZ] &= \frac{g^2 c_{\beta-\alpha}^2}{64\pi M_A c_W^2} \lambda^{1/2} \left(1, \frac{m_Z^2}{M_A^2}, \frac{M_h^2}{M_A^2} \right) \\ &\times \left[m_Z^2 - 2(M_A^2 + M_h^2) + \frac{(M_A^2 - M_h^2)^2}{m_Z^2} \right], \end{aligned} \quad (17c)$$

$$\begin{aligned} \Gamma[A \rightarrow HZ] &= \frac{g^2 s_{\beta-\alpha}^2}{64\pi M_A c_W^2} \lambda^{1/2} \left(1, \frac{m_Z^2}{M_A^2}, \frac{M_H^2}{M_A^2} \right) \\ &\times \left[m_Z^2 - 2(M_A^2 + M_H^2) + \frac{(M_A^2 - M_H^2)^2}{m_Z^2} \right], \end{aligned} \quad (17d)$$

with $N_{c,f} = 3(1)$ for quarks (leptons). The three-body phase space factor reads

$$\lambda^{1/2}(1, x^2, y^2) \equiv \left[(1 - x^2 - y^2)^2 - 4x^2 y^2 \right]^{1/2}. \quad (18)$$

For the mass-degenerate h/H scenario, one cannot discriminate two decay channels of $A \rightarrow hZ$ and $A \rightarrow HZ$ for specific final states, such as $b\bar{b} + \ell^+ \ell^-$. The signal rates for this scenario should

be evaluated as

$$\begin{aligned} \sigma_{\text{tot}} = & \sigma[pp \rightarrow AX] \times \left(\text{BR}[A \rightarrow hZ] \times \text{BR}[h \rightarrow b\bar{b}] \right. \\ & \left. + \text{BR}[A \rightarrow HZ] \times \text{BR}[H \rightarrow b\bar{b}] \right) \times \text{BR}[Z \rightarrow \ell^+ \ell^-]. \end{aligned} \quad (19)$$

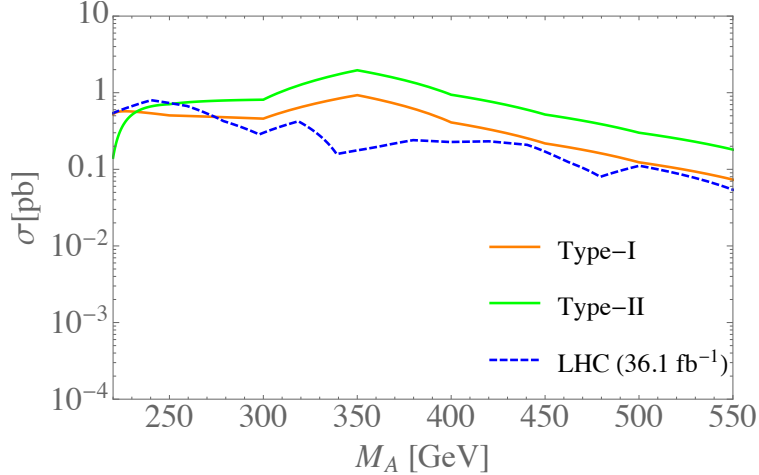


FIG. 4. The current LHC exclusion limits [70] to the h/H degenerate case through the $A \rightarrow hZ \rightarrow b\bar{b} + \ell^+ \ell^-$ final states, with an integrated luminosity of 36.1 fb^{-1} (blue dashed line). The best-fit points of $(\alpha, \beta) = (0.04, 1.40)$ for Type-I case and $(\alpha, \beta) = (-0.25, 1.31)$ for Type-II case are taken as in Table. III.

The LHC searches for a CP -odd Higgs boson via the $A \rightarrow hZ \rightarrow b\bar{b} + \ell^+ \ell^-$ were previous carried out by both ATLAS [71] and CMS [72] collaborations at the 8 TeV run. The most recent results from the ATLAS searches at the LHC 13 TeV run with integrated luminosity of 36.1 fb^{-1} is given in Ref. [70]. We estimate the production cross sections of $\sigma(gg \rightarrow A)$ at the NLO by using the package of `SusHi` [73], by using the best-fit points as in Table. III. From Fig. 4, we find that the h/H mass-degenerate scenario for either Type-I or Type-II has been tightly constrained by the current exclusion limits from the LHC 13 TeV run with an integrated luminosity of 36.1 fb^{-1} . Combining with the joint perturbative unitarity and stability bounds shown in Fig. 2, the h/H mass-degenerate scenario can still exist in the mass ranges of $M_A \lesssim 280 \text{ GeV}$ for Type-I 2HDM and $M_A \lesssim 260 \text{ GeV}$ for Type-II 2HDM, respectively. Previously, we further restrict the mass ranges of M_A in Eq. (14), in order to maximize our parameter choices of m_{12} for the Higgs pair productions. It does not mean the mass ranges of M_A in Eq. (14) are constrained by the current LHC search result. The specific mass of the CP -odd Higgs boson A will not play any role in our discussion of the future experimental tests below. On the other hand, the future searches for the CP -odd Higgs boson A via this channel at the LHC 14 TeV run will play a decisive role in justifying or falsifying this scenario.

III. THE LHC SEARCHES FOR DEGENERATE HIGGS BOSONS: CONSTRAINTS AND PAIR PRODUCTIONS

A. The total cross section of gluon-gluon fusion to Higgs pairs

By using the best-fit points in Table. III and the range of m_{12} in Eq. (14) after the set of constraints, we are ready to present the main results of the Higgs pair productions at the LHC. The cross sections we need to evaluate are

$$\sigma[gg \rightarrow hh], \quad \sigma[gg \rightarrow hH], \quad \sigma[gg \rightarrow HH], \quad (20)$$

where the individual cross section of $\sigma[gg \rightarrow h_i h_j]$ was first obtained in Ref. [74] for both SM and MSSM cases. The differential cross section at the LO reads

$$\frac{d\hat{\sigma}}{d\hat{t}} = c^{ij} \frac{G_F^2 \alpha_s^2}{256 (2\pi)^3} \left\{ \left| \sum_{q=t,b} (C_{\Delta}^{ij} F_{\Delta} + C_{\square}^{ij} F_{\square}) \right|^2 + \left| \sum_{q=t,b} C_{\square}^{ij} G_{\square} \right|^2 \right\}, \quad (21)$$

with $c^{ij} = 1/2 (1)$ for $i = j (i \neq j)$. C_{Δ} and C_{\square} represent the coefficients of the triangle and box diagrams, respectively. The Higgs cubic self couplings contribute to the C_{Δ} 's, and they read

$$C_{\Delta}^{hh} = \frac{3\lambda_{hhh} v \xi_h^q}{\hat{s} - M_h^2 + iM_h \Gamma_h} + \frac{2\lambda_{hhH} v \xi_H^q}{\hat{s} - M_H^2 + iM_H \Gamma_H}, \quad (22a)$$

$$C_{\Delta}^{hH} = \frac{2\lambda_{hhH} v \xi_h^q}{\hat{s} - M_h^2 + iM_h \Gamma_h} + \frac{2\lambda_{hHH} v \xi_H^q}{\hat{s} - M_H^2 + iM_H \Gamma_H}, \quad (22b)$$

$$C_{\Delta}^{HH} = \frac{2\lambda_{hHH} v \xi_h^q}{\hat{s} - M_h^2 + iM_h \Gamma_h} + \frac{3\lambda_{HHH} v \xi_H^q}{\hat{s} - M_H^2 + iM_H \Gamma_H}. \quad (22c)$$

The coefficients of C_{\square} are determined by the dimensionless Yukawa couplings of the Higgs bosons

$$C_{\square}^{hh} = (\xi_h^q)^2, \quad C_{\square}^{hH} = \xi_h^q \xi_H^q, \quad C_{\square}^{HH} = (\xi_H^q)^2, \quad (23)$$

for $q = (t, b)$. The form factors of the triangle and box diagrams ($F_{\Delta}, F_{\square}, G_{\square}$) in Eq. (21) can be found in the Appendix of Ref. [74]. The asymptotic behaviors of these form factors in the large quark mass and small quark mass limits read

$$m_q^2 \gg \hat{s} : F_{\Delta} \simeq \frac{2}{3} + \mathcal{O}\left(\frac{\hat{s}}{m_q^2}\right), \quad F_{\square} \simeq -\frac{2}{3} + \mathcal{O}\left(\frac{\hat{s}}{m_q^2}\right), \quad G_{\square} \simeq \mathcal{O}\left(\frac{\hat{s}}{m_q^2}\right), \quad (24a)$$

$$m_q^2 \ll \hat{s} : F_{\Delta} \simeq -\frac{m_q^2}{\hat{s}} \left[\log\left(\frac{m_q^2}{\hat{s}}\right) + i\pi \right]^2 + \mathcal{O}\left(\frac{m_q^2}{\hat{s}}\right), \quad F_{\square}, G_{\square} \simeq \mathcal{O}\left(\frac{m_q^2}{\hat{s}}\right). \quad (24b)$$

In practice, we evaluate the corresponding Passarino-Veltman (PV) integrals are evaluated by using the `LoopTools` package [75].

At the LHC, the differential cross section in the lab frame is obtained by convoluting the parton-level cross section in Eq. (21) with the gluon PDFs

$$\frac{d^2\sigma}{dM_{hh} dp_T} = \int_{\tau}^1 \frac{dx}{x} f_g(x, \mu_F) f_g\left(\frac{\tau}{x}, \mu_F\right) \frac{2M_{hh}}{s} \frac{d\hat{\sigma}}{dp_T}, \quad (25)$$

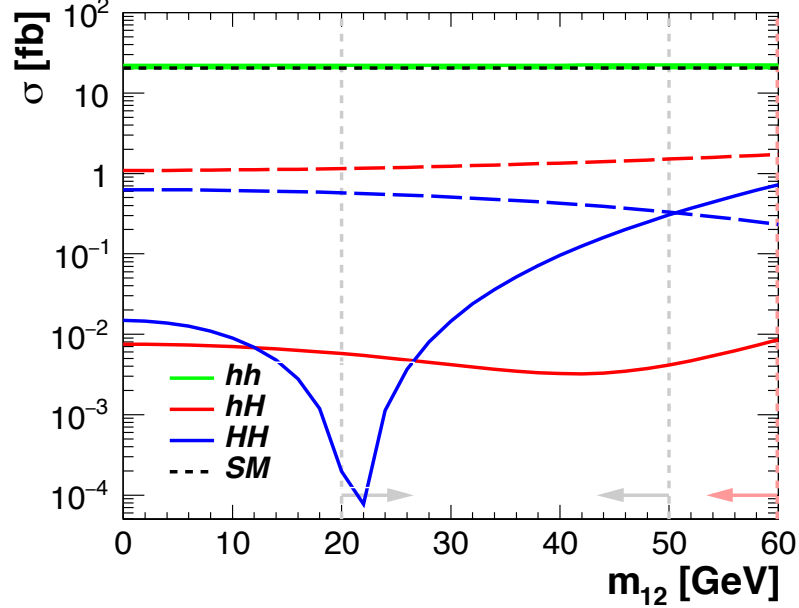


FIG. 5. The LO cross sections of $\sigma[gg \rightarrow hh]$ (green), $\sigma[gg \rightarrow hH]$ (red), and $\sigma[gg \rightarrow HH]$ (blue) versus the soft mass m_{12} in both Type-I (solid) and Type-II (dashed) 2HDM at the LHC $\sqrt{s} = 14$ TeV run. The best-fit points of $(\alpha, \beta) = (0.04, 1.40)$ for Type-I case and $(\alpha, \beta) = (-0.25, 1.31)$ for Type-II case are taken as in Table. III. In comparison, the LO cross section of $\sigma[gg \rightarrow h_{\text{SM}}h_{\text{SM}}] = 20.5$ fb (black dotted) is listed as well. Note that the allowed regions obtained from theoretical constraints in m_{12} are also indicated by the gray and pink arrows for Type-I and Type-II respectively.

where s is the squared center-of-mass energy at the LHC, M_{hh} is the invariant mass of the Higgs pairs, $\tau = M_{hh}^2/s$, and p_T denotes the transverse momentum of the Higgs boson. In practice, we use the LO MSTW PDF [76] for the evaluation. The LO cross sections of individual production mode of $\sigma[gg \rightarrow hh]$, $\sigma[gg \rightarrow hH]$, and $\sigma[gg \rightarrow HH]$ are displayed in Fig. 5, with the renormalization and factorization scale set to be $\mu_R = \mu_F = M_{hh}$. The cross sections of $\sigma[gg \rightarrow hh]$ are very close to the corresponding SM predicted value, as stated previously. The contributions from $\sigma[gg \rightarrow hH]$ and $\sigma[gg \rightarrow HH]$ are sub-leading ones, yet they play a role in determining the signal rates. A dip is shown in the cross section of $\sigma[gg \rightarrow hH]$ versus m_{12} , which roughly matches the position where the Higgs cubic self coupling λ_{hHH} flips sign. The next-to-leading order contributions to the Higgs pair productions at the LHC are known to be significant [77–81]. Our estimation below focus on the future experimental significances via various channels, where a same K -factor can be assumed for both h/H mass-degenerate case and the SM Higgs boson case, as in Ref. [82]. Therefore, the LO results are sufficient for our estimation below.

B. The cross sections of Higgs pairs to various final states

Next, we proceed to present the cross sections of the Higgs pairs to specific final states with the mass-degenerate Higgs benchmark points in Table III. Two leading final states of $4b$ and $2b2\gamma$ will be taken into account [83]. The signal rates are estimated as follows

$$\begin{aligned} \sigma[gg \rightarrow (hh, hH, HH) \rightarrow (XXYY)] &= \sigma[gg \rightarrow hh](\kappa_{XY}\text{Br}[h \rightarrow XX]\text{Br}[h \rightarrow YY]) \\ &+ \sigma[gg \rightarrow hH](\text{Br}[h \rightarrow XX]\text{Br}[H \rightarrow YY] + (h \leftrightarrow H)) \\ &+ \sigma[gg \rightarrow HH](\kappa_{XY}\text{Br}[H \rightarrow XX]\text{Br}[H \rightarrow YY]), \end{aligned} \quad (26)$$

with $\kappa_{XY} = 1$ (2) for $X = Y$ ($X \neq Y$). For a single SM-like Higgs boson with mass ~ 125 GeV, the ratio of signal rates between the $4b$ and $2b2\gamma$ final states is fixed to be $\sigma[4b] : \sigma[2b2\gamma] \approx 127 : 1$. This always holds, no matter how one modifies the SM-like Higgs cubic self couplings and includes the additional resonance contributions. We find the ratios of signal rates between these two channels are generally different from the single SM-like Higgs boson case, which reads $\sigma[4b] : \sigma[2b2\gamma] \approx 140 : 1$ with $m_{12} = 50$ GeV in the Type-I case, and $\sigma[4b] : \sigma[2b2\gamma] \approx 129 : 1$ with $m_{12} = 60$ GeV in the Type-II case.

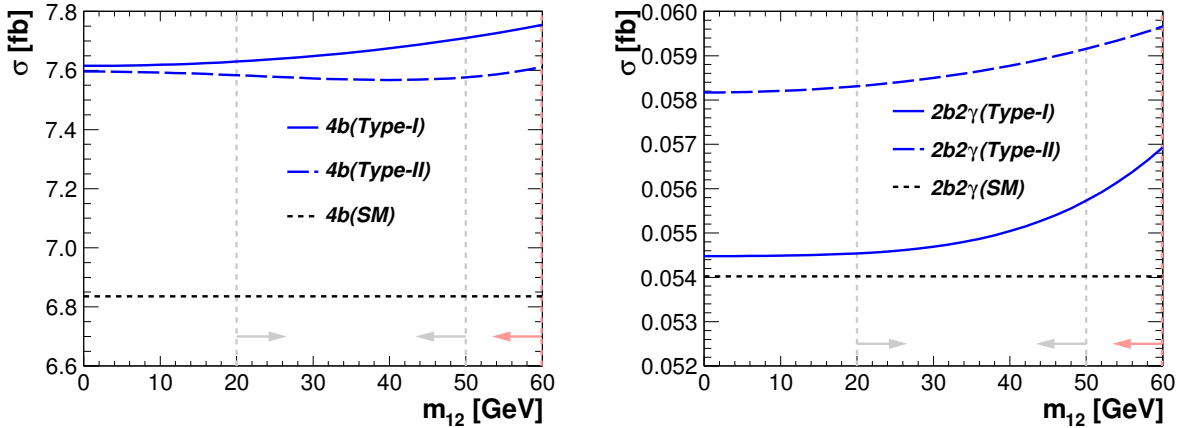


FIG. 6. The LHC 14 TeV LO cross sections of $\sigma[gg \rightarrow (hh, hH, HH)]$ to final states of $4b$ (left panel) and $2b2\gamma$ (right panel) versus the soft mass m_{12} in the Type-I (solid lines) and Type-II (dashed lines) 2HDM. The best-fit points of $(\alpha, \beta) = (0.04, 1.40)$ for Type-I case and $(\alpha, \beta) = (-0.25, 1.31)$ for Type-II case are taken as in Table. III. In comparison, the LO cross sections of $\sigma[gg \rightarrow h_{\text{SM}}h_{\text{SM}}]$ to the corresponding final states (dotted lines) are displayed as well. Note that the allowed regions obtained from theoretical constraints in m_{12} are also indicated by the gray and pink arrows for Type-I and Type-II respectively.

The LHC 14 TeV cross sections for $\sigma[gg \rightarrow (hh, hH, HH) \rightarrow (4b, 2b2\gamma)]$ final states versus the soft mass term m_{12} are shown in Fig. 6. We find enhancements of both $4b$ and $2b2\gamma$ signal rates, in comparison to the SM Higgs boson pair productions. This kind of enhancements were previously investigated in Ref. [84]. However, the parameter region of m_{12} is severely restricted

by the theoretical constraints as shown in Fig. 2. The LO cross sections for the $4b$ final states are moderately enhanced to ~ 7.7 fb with $m_{12} = 50$ GeV in the Type-I case, or ~ 7.6 fb with $m_{12} = 60$ GeV in the Type-II case. The corresponding LO cross section for the $4b$ channel in the SM is $\simeq 6.8$ fb. By extrapolating the current LHC run-II results from 13 TeV, the ATLAS and CMS give conservative estimations to the significances for the SM Higgs boson pairs at the HL LHC runs as [83]

$$\begin{aligned} \text{ATLAS :} & \quad 1.05 \sigma \quad \text{for} \quad 2b2\gamma \\ \text{CMS :} & \quad (0.39 \sigma, 1.6 \sigma) \quad \text{for} \quad (4b, 2b2\gamma) \end{aligned} \tag{27}$$

We summarize the significance of the Type-I and Type-II h/H mass-degenerate Higgs boson pairs via the $4b$ and $2b2\gamma$ channels in Table. IV. We note that the current LHC run-II results are not optimal for the HL-LHC runs, future improvements to the significance via the $2b2\gamma$ channel should be expected.

	$4b$	$2b2\gamma$
Type-I (m_{12})	$\sim 0.44 \sigma (20 - 50 \text{ GeV})$	$1.61 \sigma (20 \text{ GeV}) \quad 1.64 \sigma (50 \text{ GeV})$
Type-II (m_{12})	$\sim 0.43 \sigma (0 - 60 \text{ GeV})$	$1.71 \sigma (0 \text{ GeV}) \quad 1.75 \sigma (60 \text{ GeV})$

TABLE IV. The significances of the h/H mass-degenerate Higgs boson pair production measurements via the $4b$ and $2b2\gamma$ channels at the HL-LHC.

IV. PROBES OF DEGENERATE HIGGS BOSONS AT THE e^+e^- COLLIDERS

The future plans of the high-energy e^+e^- colliders include the CEPC [85], ILC [86], and TLEP [87]. They will play a role as Higgs factory to produce millions of SM-like Higgs bosons for the precise measurements, with the running at center-of-mass energy of $\sqrt{s} = 250$ GeV, which will provide excellent opportunity for us to examine the Higgs properties in many NP models [88]. It was pointed out in Ref. [89] that the precise measurement of the Higgs production cross section at the CEPC or ILC is sensitive to the Higgs self couplings at the NLO. At the ILC, it is likely to upgrade the center-of-mass energy up to $\sqrt{s} = 500$ GeV, so that it can directly produce 125 GeV Higgs boson pairs associated with a Z -boson.

A. The CEPC measurements of the degenerate Higgs scenario

The circular electron-positron collider (CEPC) will operate at the center-of-mass energy of $\sqrt{s} = 250$ GeV. A key physical goal of CEPC is to measure the Higgs boson mass precisely, which can be as small as ~ 5.9 MeV with an integrated luminosity of 5 ab^{-1} . The precision on $\sigma(ZH)$

is about 0.51% combining all decay modes for the Z -boson with the same luminosity [85]. The resolution for the recoil mass peak measurement is about 400 MeV for ILC [90–92].

With the integrated luminosity of 5 ab^{-1} , CEPC can measure the cross section of $\sigma[e^+e^- \rightarrow hZ]$ with an accuracy of $\sim 0.51\%$ [85], by combining both the leptonic and hadronic decay modes of Z -bosons. The LO cross section of the SM Higgs boson production associated with Z -boson at the CEPC reads $\sigma[e^+e^- \rightarrow h_{\text{SM}}Z] \simeq 221.54 \text{ fb}$ ⁶. The cross sections for the best-fit points in Table. III are $\sigma[e^+e^- \rightarrow hZ] \simeq 211.55 \text{ fb}$ and $\sigma[e^+e^- \rightarrow HZ] \simeq 9.99 \text{ fb}$ for the Type-I case, $\sigma[e^+e^- \rightarrow hZ] \simeq 221.52 \text{ fb}$ and $\sigma[e^+e^- \rightarrow HZ] \simeq 0.02 \text{ fb}$ for the Type-II case. Combined with the leading decay modes in Table. III, we have $\sigma[e^+e^- \rightarrow h(\rightarrow b\bar{b})Z] \simeq 124.65 \text{ fb}$ and $\sigma[e^+e^- \rightarrow H(\rightarrow b\bar{b})Z] \simeq 0.26 \text{ fb}$ for the Type-I case, or $\sigma[e^+e^- \rightarrow h(\rightarrow b\bar{b})Z] \simeq 124.87 \text{ fb}$ and $\sigma[e^+e^- \rightarrow H(\rightarrow b\bar{b})Z] \simeq 1.8 \times 10^{-2} \text{ fb}$ for the Type-II case. Due to the jet energy resolutions, one does not expect to distinguish two separate peaks from two mass-degenerate Higgs bosons, with mass split of $\sim 0.1 \text{ GeV}$. Instead, the inclusive cross sections of h/H mass-degenerate Higgs bosons with $b\bar{b}$ final states are about $\sim 2\%$ lower than the SM predicted values for both Type-I and Type-II cases. Compared with $\sim 0.28\%$ precision that could be achieved at CEPC [85], there will be roughly 7σ deviation. Therefore, a decrease of the cross section for the $\sigma[e^+e^- \rightarrow hZ]$ will be a first indication from the best-fit points in Table. III.

B. The direct probes of the degenerate Higgs scenario at the ILC

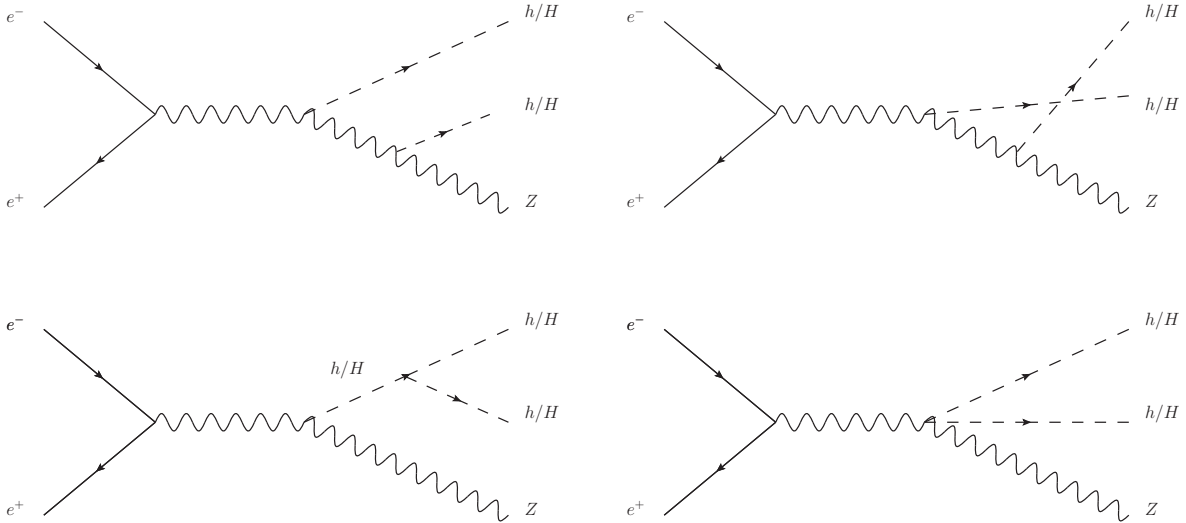


FIG. 7. The Feynman diagrams for the Higgs boson pair productions associated with a Z -boson at the ILC.

The ILC can directly produce Higgs boson pairs associated with a Z -boson, when it runs at the

⁶ See Refs. [93–97] for more precisely prediction including higher order corrections.

center-of-mass energy of $\sqrt{s} = 500$ GeV. The Feynman diagrams for the corresponding processes are depicted in Fig. 7. The cross sections at the ILC can be expressed as [98]

$$\sigma = \frac{1}{4} \left[(1 + P_{e^-})(1 + P_{e^+})\sigma_{\text{RR}} + (1 - P_{e^-})(1 - P_{e^+})\sigma_{\text{LL}} \right. \\ \left. + (1 + P_{e^-})(1 - P_{e^+})\sigma_{\text{RL}} + (1 - P_{e^-})(1 + P_{e^+})\sigma_{\text{LR}} \right], \quad (28)$$

where σ_{LR} denotes the cross section at beam polarization configurations of $(P_{e^+}, P_{e^-}) = (+1, -1)$, and etc. The ILC will run at $\sqrt{s} = 500$ GeV with an integrated luminosity of 4 ab^{-1} , which will be equally shared by two beam polarization configurations of $(P_{e^+}, P_{e^-}) = (\pm 0.3, \mp 0.8)$ [86, 99]. The corresponding cross sections for the $e^+e^- \rightarrow hhZ$ read

$$\sigma_{(+0.3, -0.8)} = 0.585 \sigma_{\text{LR}} + 0.035 \sigma_{\text{RL}}, \quad (29\text{a})$$

$$\sigma_{(-0.3, +0.8)} = 0.035 \sigma_{\text{LR}} + 0.585 \sigma_{\text{RL}}. \quad (29\text{b})$$

$P(e^+, e^-)$	Channel	Excess significance	Precision on σ_{ZHH}
(0.3,-0.8)	$HH \rightarrow b\bar{b}b\bar{b}$	3.5σ	30.3%
(-0.3,0.8)	$HH \rightarrow b\bar{b}b\bar{b}$	4.8σ	29.4%
(0.0,-0.8)	$HH \rightarrow b\bar{b}b\bar{b}$	3.5σ	34.7%
(0.0,0.8)	$HH \rightarrow b\bar{b}b\bar{b}$	4.2σ	33.7%
(0.6,-0.8)	$HH \rightarrow b\bar{b}b\bar{b}$	4.2σ	28.7%
(-0.6,0.8)	$HH \rightarrow b\bar{b}b\bar{b}$	5.5σ	27.8%
(0.3,-0.8)	$HH \rightarrow b\bar{b}W^+W^-$	1.91σ	...

TABLE V. The prospects of measuring the Higgs pair productions at the ILC. For each beam polarization configuration, an integrated luminosity of $\mathcal{L} = 2 \text{ ab}^{-1}$ is assumed.

Prospects of measuring the cross sections of the SM Higgs boson pair production via the $hh \rightarrow b\bar{b}b\bar{b}$ and $hh \rightarrow b\bar{b}W^+W^-$ final states have been investigated in Refs. [100, 101]. The corresponding significance are listed in Table. V. Combining these measurements for $(P_{e^+}, P_{e^-}) = (\pm 0.3, \mp 0.8)$, we obtain the ILC precision on the measurement of $(\sigma_{\text{RL}}, \sigma_{\text{LR}})$ in Fig. 8, with two contours for 1- and 2- σ regions, respectively. In Fig. 8, we also show the best-fit points for Type-I (Black) and Type-II (Red) 2HDM in the same plane. Each point represents different value of m_{12} given by the corresponding label. Note that the 2HDM cross sections are calculated by using the best-fit points in the (α, β) plane from the LHC global fitting in previous section. From Fig. 8, we find that for the h/H mass-degenerate Type-I 2HDM case, the cross sections for all allowed m_{12} are still within the precision of the ILC measurement. However, the h/H mass-degenerate Type-II 2HDM points can be excluded from the Higgs pair production measurements at the ILC.

More details can be found in Fig. 9, where we combine $hh \rightarrow b\bar{b}b\bar{b}$ and $hh \rightarrow b\bar{b}W^+W^-$ channels and use the log-likelihood ratio method to perform the hypothesis test against the SM predictions. The exclusion levels for different m_{12} values are presented by the black and red line in the left

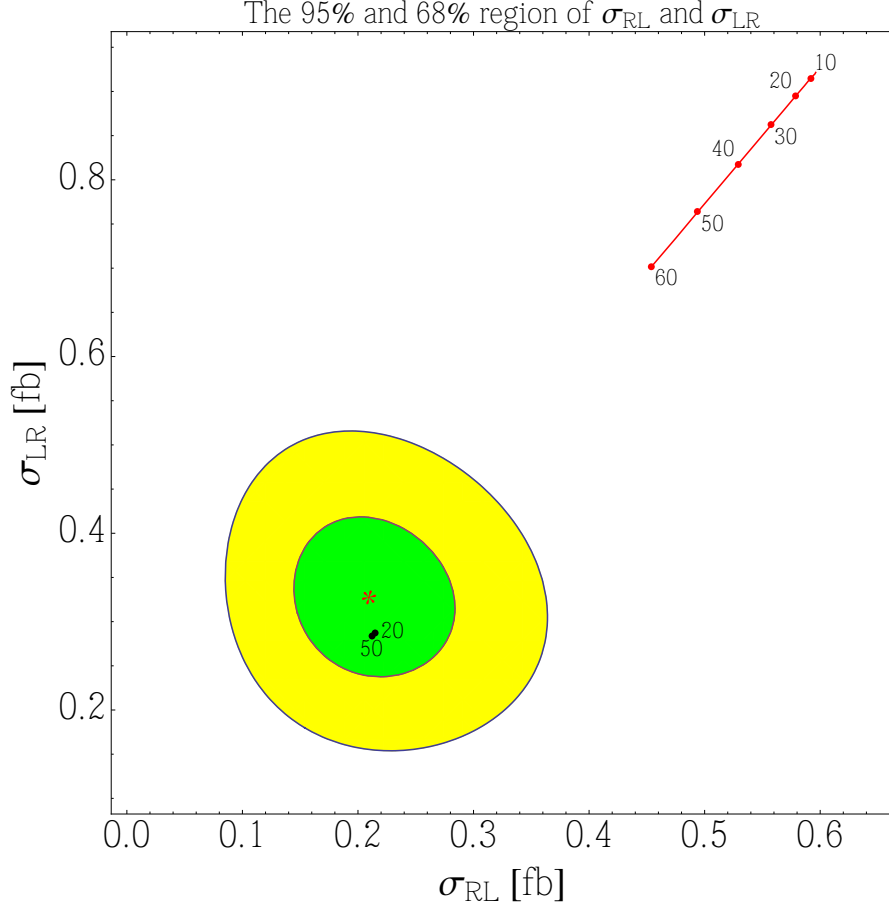


FIG. 8. 95% and 68% contours of the measurement of $\sigma_{ZH,LR}$ and $\sigma_{ZH,RL}$ from (1) $hh \rightarrow b\bar{b}b\bar{b}$ with $P(e^-, e^+) = (\pm 0.8, \mp 0.3)$ [100] and (2) $hh \rightarrow b\bar{b}W^+W^-$ with $P(e^-, e^+) = (-0.8, 0.3)$ [101] for 500 GeV ILC with 2 ab^{-1} luminosity for each beam polarization configuration. The best-fit points of $(\alpha, \beta) = (0.04, 1.40)$ for Type-I case and $(\alpha, \beta) = (-0.25, 1.31)$ for Type-II case are taken as in Table. III. The tiny black line represents the prediction of the cross section (normalized according to the branching fraction) of Type-I with variation of m_{12} , the red line is for Type-II. The label beside each point indicates the value of corresponding m_{12} .

panel for Type-I and Type-II cases, respectively. Dashed vertical lines with arrows indicate the allowed region from 2HDM potential unitarity/stability constraints. We find that for Type-II case, the theoretical allowed region of m_{12} has already been excluded by the ILC measurement at 4σ or more, with 2 ab^{-1} luminosity for each beam polarization configuration. In contrast, the allowed region for the Type-I case is still safely sitting within 1σ region of the ILC measurement. In the right panel, we present the exclusion level as a function of the luminosity cumulated at the ILC for beam polarization configurations of $P(e^-, e^+) = (\pm 0.8, \mp 0.3)$. The black and red line are for Type-I and Type-II case, respectively. For illustration, we choose the most sensitive value of m_{12} in the stability allowed region for each type: $m_{12} = 50$ (0) GeV for Type-I (Type-II). We can see that,

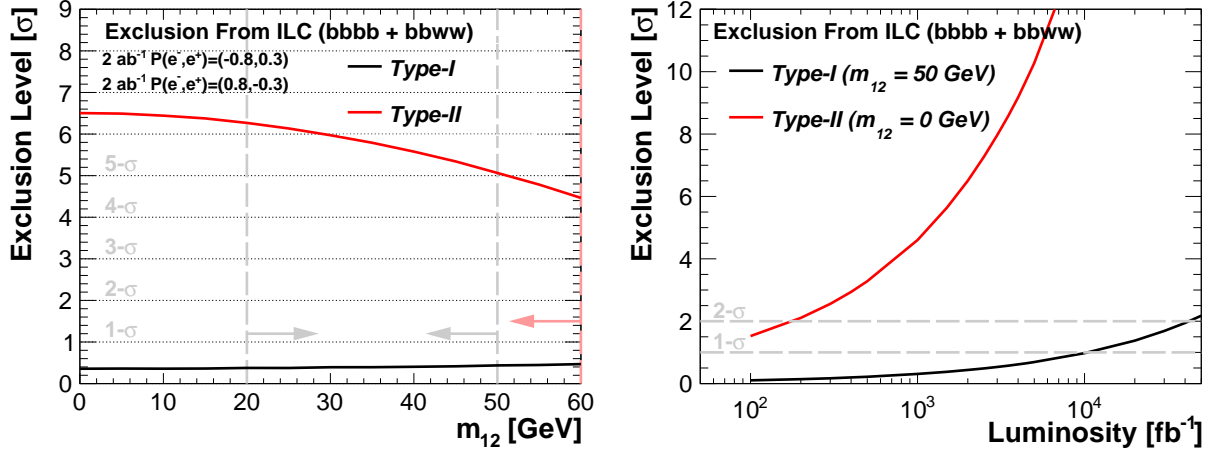


FIG. 9. Left: the exclusion level of the hypothesis test of the 2HDM model against SM using $hh \rightarrow bbbb$ and $hh \rightarrow bbWW$ channels with $(P_{e^+}, P_{e^-}) = (\pm 0.3, \mp 0.8)$ and 2 ab^{-1} luminosity for each polarization states. The black (red) line represents the exclusion level for the h/H degenerate in the Type-I (Type-II) 2HDM with dependence on m_{12} . The gray and red vertical dashed lines with arrow directions in the left panel indicate the allowed upper bounds from the 2HDM potential stability constraints for Type-I and Type-II, respectively. Right: the exclusion level the same as in the left panel, but with dependence on the luminosity cumulated for each beam polarization configuration, $m_{12} = 50$ (0) GeV is used for Type-I (Type-II) for presentation.

the ILC has sensitivity to Type-II in this case when an integrated luminosity of 400 fb^{-1} (equally shared by two beam polarization configurations) is cumulated. However, at least an integrated luminosity of 80 ab^{-1} is required for the ILC to be sensitive to the Type-I in this situation, which is unrealistic.

V. CONCLUSION

In this work, we study the future prospects of distinguishing the mass-degenerate Higgs boson scenario from the single resonance case at the LHC and future e^+e^- colliders. Our study is performed in the general CPC 2HDM framework, with two CP -even Higgs bosons of h/H to be mass-degenerate. The direct measurements of the Higgs boson signal rates at the 125 GeV only probe its/their gauge couplings and Yukawa couplings. Alternatively, we find this scenario can be further constrained by a series of theoretical bounds and direct experimental searches in such a framework. Moreover, we suggest that the study of the Higgs boson pair productions will be useful for this scenario. Specifically, there are four types of Higgs cubic self couplings involved in the Higgs pair productions, which are $(\lambda_{hhh}, \lambda_{hhH}, \lambda_{hHH}, \lambda_{HHH})$. The physical processes to be considered are the ggF to Higgs boson pair productions at the LHC, and the Higgs boson pair productions associated with a Z -boson at the ILC.

By performing the global fit of the LHC measurements of the 125 GeV Higgs boson signal rates, we find the best-fit points with mass-degenerate h/H in Type-I and Type-II 2HDM in (α, β) plane. The best-fit point in the Type-I case deviate from the alignment limit as large as $c_{\beta-\alpha} \simeq 0.21$, while it approaches to the alignment limit as $c_{\beta-\alpha} \sim \mathcal{O}(10^{-2})$ in the Type-II case. Correspondingly, one Higgs boson H becomes almost gaugephobic in the Type-II case. The h/H mass-degenerate scenario also passes the current LHC run-II searches for the CP -odd Higgs boson A via the $b\bar{b} + \ell^+\ell^-$ final states. Meanwhile, it also means that the further LHC searches for the CP -odd Higgs boson A below the $t\bar{t}$ mass threshold will play a role to justify or falsify the h/H mass-degenerate scenario.

The relevant cubic Higgs self couplings, such as λ_{hHH} and λ_{HHH} , are not vanishing even when the 2HDM parameters approach to the alignment limit. This suggests that the Higgs pair production processes can crucial to justify or falsify the h/H mass-degenerate scenario. The signal predictions of the ggF to mass-degenerate Higgs boson pairs are made at the LHC 14 TeV runs, with the focus on two leading search channels of $4b$ and $2b2\gamma$. Moderate signal enhancements with respect to the SM predictions are expected, while the enhancements are at most $\sim 10\%$. Therefore, the Higgs boson pair productions at the LHC are less likely to probe the h/H mass-degenerate scenario. At the ILC 500 GeV run, we find that the h/H mass-degenerate samples in the Type-I case are within the precision of the ILC measurement, while the h/H mass-degenerate samples in the Type-II case can be probed or excluded with an integrated luminosity of 400 fb^{-1} . It means that the ILC 500 GeV run offers an opportunity to fully probe the h/H mass-degenerate scenario in the Type-II case.

Though our predictions are model-dependent, the Higgs pair productions with two mass-degenerate Higgs bosons can be generalized to any other NP models with multiple Higgs bosons. There are multiple Higgs self couplings involved in the Higgs pair productions in general. Depending on the model setup, these self-couplings may be bounded by the constraints mentioned in the current study. Our discussion through the context focus on the ggF process at the LHC and the Higgs pair strahlung at the ILC. This discussion can be extended to other Higgs pair production channels, including the vector boson fusion (VBF) and $t\bar{t}$ associated processes at the future high-energy e^+e^- and pp colliders.

ACKNOWLEDGMENTS

We would like to thank Yanwen Liu, Zuowei Liu, Manqi Ruan, and Junping Tian for very useful discussions and communication. The work of N.C. is partially supported by the National Natural Science Foundation of China (under Grant No. 11575176) and Center for Future High Energy Physics (CFHEP). The work of L.G.B. is partially supported by the National Natural Science Foundation of China (under Grant No. 11605016), Basic Science Research Program through the National Research Foundation of Korea (NRF) funded by the Ministry of Education, Science and Technology (NRF-2016R1A2B4008759), and Korea Research Fellowship Program through the National Research Foundation of Korea (NRF) funded by the Ministry of Science and ICT (2017H1D3A1A01014046). The work of Y.C.W is partially supported by the Natural Sciences and

Engineering Research Council of Canada. The work of Y.Z. is partially supported by the National Natural Science Foundation of China (under Grant Nos. of 11775109 and U1738134), by he Nanjing University (under Grant No.14902303), the China Postdoctoral Science Foundation (under Grant No. 2017M611771), and the Fundamental Research Funds for the Central Universities (under Grant No. 020414380097). N.C. would like to thank Nanjing University for their hospitalities when part of this work was prepared.

-
- [1] Georges Aad et al. Observation of a new particle in the search for the Standard Model Higgs boson with the ATLAS detector at the LHC. *Phys. Lett.*, B716:1–29, 2012.
- [2] Serguei Chatrchyan et al. Observation of a new boson at a mass of 125 GeV with the CMS experiment at the LHC. *Phys. Lett.*, B716:30–61, 2012.
- [3] John F. Gunion, Yun Jiang, and Sabine Kraml. Could two NMSSM Higgs bosons be present near 125 GeV? *Phys. Rev.*, D86:071702, 2012.
- [4] John F. Gunion, Yun Jiang, and Sabine Kraml. Diagnosing Degenerate Higgs Bosons at 125 GeV. *Phys. Rev. Lett.*, 110(5):051801, 2013.
- [5] P. M. Ferreira, Rui Santos, Howard E. Haber, and Joao P. Silva. Mass-degenerate Higgs bosons at 125 GeV in the two-Higgs-doublet model. *Phys. Rev.*, D87:055009, 2013.
- [6] M. Chabab, M. C. Peyranere, and L. Rahili. Degenerate Higgs bosons decays to $\gamma\gamma$ and $Z\gamma$ in the type II seesaw model. *Phys. Rev.*, D90(3):035026, 2014.
- [7] Nathaniel Craig, Jamison Galloway, and Scott Thomas. Searching for Signs of the Second Higgs Doublet. 2013.
- [8] Ning Chen and Zuowei Liu. Degenerate Higgs bosons: hiding a second Higgs at 125 GeV. 2016.
- [9] Biswaranjan Das, Stefano Moretti, Shoaib Munir, and Poulouse Poulouse. Two Higgs bosons near 125 GeV in the NMSSM: beyond the narrow width approximation. *Eur. Phys. J.*, C77(8):544, 2017.
- [10] Georges Aad et al. Electron and photon energy calibration with the ATLAS detector using LHC Run 1 data. *Eur. Phys. J.*, C74(10):3071, 2014.
- [11] Georges Aad et al. Measurement of the muon reconstruction performance of the ATLAS detector using 2011 and 2012 LHC proton–proton collision data. *Eur. Phys. J.*, C74(11):3130, 2014.
- [12] Serguei Chatrchyan et al. Performance of CMS muon reconstruction in pp collision events at $\sqrt{s} = 7$ TeV. *JINST*, 7:P10002, 2012.
- [13] Vardan Khachatryan et al. Performance of Electron Reconstruction and Selection with the CMS Detector in Proton-Proton Collisions at $\sqrt{s} = 8$ TeV. *JINST*, 10(06):P06005, 2015.
- [14] Vardan Khachatryan et al. Performance of Photon Reconstruction and Identification with the CMS Detector in Proton-Proton Collisions at $\sqrt{s} = 8$ TeV. *JINST*, 10(08):P08010, 2015.
- [15] Serguei Chatrchyan et al. Study of the Mass and Spin-Parity of the Higgs Boson Candidate Via Its Decays to Z Boson Pairs. *Phys. Rev. Lett.*, 110(8):081803, 2013.
- [16] Vardan Khachatryan et al. Precise determination of the mass of the Higgs boson and tests of compatibility of its couplings with the standard model predictions using proton collisions at 7 and 8 TeV. *Eur. Phys. J.*, C75(5):212, 2015.
- [17] Jia Liu, Xiao-Ping Wang, and Shou-hua Zhu. Discovering extra Higgs boson via pair production of the SM-like Higgs bosons. 2013.

- [18] Ligong Bian and Ning Chen. Higgs pair productions in the CP-violating two-Higgs-doublet model. *JHEP*, 09:069, 2016.
- [19] Giacomo Cacciapaglia, Haiying Cai, Alexandra Carvalho, Aldo Deandrea, Thomas Flacke, Benjamin Fuks, Devdatta Majumder, and Hua-Sheng Shao. Probing vector-like quark models with Higgs-boson pair production. *JHEP*, 07(7):005, 2017.
- [20] R. Grober, M. Muhlleitner, and M. Spira. Higgs Pair Production at NLO QCD for CP-violating Higgs Sectors. *Nucl. Phys.*, B925:1–27, 2017.
- [21] G. Chalons, A. Djouadi, and J. Quevillon. The neutral Higgs self-couplings in the (h)MSSM. *Phys. Lett.*, B780:74–80, 2018.
- [22] S. Dawson and M. Sullivan. Enhanced di-Higgs boson production in the complex Higgs singlet model. *Phys. Rev.*, D97(1):015022, 2018.
- [23] Philipp Basler, Margarete Mühlleitner, and Jonas Wittbrodt. The CP-Violating 2HDM in Light of a Strong First Order Electroweak Phase Transition and Implications for Higgs Pair Production. *JHEP*, 03:061, 2018.
- [24] The ATLAS collaboration. Search for pair production of Higgs bosons in the $b\bar{b}b\bar{b}$ final state using proton–proton collisions at $\sqrt{s} = 13$ TeV with the ATLAS detector. 2016.
- [25] CMS Collaboration. Search for resonant pair production of Higgs bosons decaying to two bottom quark-antiquark pairs in proton-proton collisions at 13 TeV. 2016.
- [26] CMS Collaboration. Search for resonant Higgs boson pair production in the $b\bar{b}l\nu l\nu$ final state at $\sqrt{s} = 13$ TeV. 2016.
- [27] CMS Collaboration. Search for pair production of Higgs bosons in the two tau leptons and two bottom quarks final state using proton-proton collisions at $\sqrt{s} = 13$ TeV. 2017.
- [28] The ATLAS collaboration. Search for Higgs boson pair production in the $b\bar{b}\gamma\gamma$ final state using pp collision data at $\sqrt{s} = 13$ TeV with the ATLAS detector. 2016.
- [29] CMS Collaboration. Search for H(bb)H(gammagamma) decays at 13TeV. 2016.
- [30] G. C. Branco, P. M. Ferreira, L. Lavoura, M. N. Rebelo, Marc Sher, and Joao P. Silva. Theory and phenomenology of two-Higgs-doublet models. *Phys. Rept.*, 516:1–102, 2012.
- [31] Georges Aad et al. Measurement of Higgs boson production in the diphoton decay channel in pp collisions at center-of-mass energies of 7 and 8 TeV with the ATLAS detector. *Phys. Rev.*, D90(11):112015, 2014.
- [32] Vardan Khachatryan et al. Observation of the diphoton decay of the Higgs boson and measurement of its properties. *Eur. Phys. J.*, C74(10):3076, 2014.
- [33] Georges Aad et al. Measurements of Higgs boson production and couplings in the four-lepton channel in pp collisions at center-of-mass energies of 7 and 8 TeV with the ATLAS detector. *Phys. Rev.*, D91(1):012006, 2015.

- [34] Serguei Chatrchyan et al. Measurement of the properties of a Higgs boson in the four-lepton final state. *Phys. Rev.*, D89(9):092007, 2014.
- [35] Georges Aad et al. Observation and measurement of Higgs boson decays to WW^* with the ATLAS detector. *Phys. Rev.*, D92(1):012006, 2015.
- [36] Serguei Chatrchyan et al. Measurement of Higgs boson production and properties in the WW decay channel with leptonic final states. *JHEP*, 01:096, 2014.
- [37] Georges Aad et al. Search for the Standard Model Higgs boson produced in association with top quarks and decaying into $b\bar{b}$ in pp collisions at $\sqrt{s} = 8$ TeV with the ATLAS detector. *Eur. Phys. J.*, C75(7):349, 2015.
- [38] Vardan Khachatryan et al. Search for a Standard Model Higgs Boson Produced in Association with a Top-Quark Pair and Decaying to Bottom Quarks Using a Matrix Element Method. *Eur. Phys. J.*, C75(6):251, 2015.
- [39] Georges Aad et al. Search for the $b\bar{b}$ decay of the Standard Model Higgs boson in associated $(W/Z)H$ production with the ATLAS detector. *JHEP*, 01:069, 2015.
- [40] Serguei Chatrchyan et al. Search for the standard model Higgs boson produced in association with a W or a Z boson and decaying to bottom quarks. *Phys. Rev.*, D89(1):012003, 2014.
- [41] Georges Aad et al. Evidence for the Higgs-boson Yukawa coupling to tau leptons with the ATLAS detector. *JHEP*, 04:117, 2015.
- [42] Serguei Chatrchyan et al. Evidence for the 125 GeV Higgs boson decaying to a pair of τ leptons. *JHEP*, 05:104, 2014.
- [43] The ATLAS collaboration. Measurements of Higgs boson properties in the diphoton decay channel with 36.1 fb^{-1} pp collision data at the center-of-mass energy of 13 TeV with the ATLAS detector. 2017.
- [44] The ATLAS collaboration. Combined measurements of Higgs boson production and decay in the $H \rightarrow ZZ^* \rightarrow 4\ell$ and $H \rightarrow \gamma\gamma$ channels using $\sqrt{s} = 13$ TeV pp collision data collected with the ATLAS experiment. 2017.
- [45] CMS Collaboration. Measurements of properties of the Higgs boson decaying into four leptons in pp collisions at $\sqrt{s} = 13$ TeV. 2017.
- [46] The ATLAS collaboration. Measurement of the Higgs boson coupling properties in the $H \rightarrow ZZ^* \rightarrow 4\ell$ decay channel at $\sqrt{s} = 13$ TeV with the ATLAS detector. 2017.
- [47] Albert M Sirunyan et al. Measurements of properties of the Higgs boson decaying into the four-lepton final state in pp collisions at $\sqrt{s} = 13$ TeV. *JHEP*, 11:047, 2017.
- [48] CMS Collaboration. Higgs to WW measurements with 15.2 fb^{-1} of 13 TeV proton-proton collisions. 2017.
- [49] The ATLAS collaboration. Measurements of the Higgs boson production cross section via Vector Boson Fusion and associated WH production in the $WW^* \rightarrow \ell\nu\ell\nu$ decay mode with the ATLAS detector at

- $\sqrt{s} = 13$ TeV. 2016.
- [50] M. Aaboud et al. Evidence for the $H \rightarrow b\bar{b}$ decay with the ATLAS detector. *JHEP*, 12:024, 2017.
 - [51] Albert M Sirunyan et al. Observation of the Higgs boson decay to a pair of τ leptons with the CMS detector. *Phys. Lett.*, B779:283–316, 2018.
 - [52] CMS Collaboration. Search for the associated production of a Higgs boson with a top quark pair in final states with a τ lepton at $\sqrt{s} = 13$ TeV. 2017.
 - [53] A. Abdesselam et al. Measurement of the inclusive $B \rightarrow X_{s+d}\gamma$ branching fraction, photon energy spectrum and HQE parameters. In *Proceedings, 38th International Conference on High Energy Physics (ICHEP 2016): Chicago, IL, USA, August 3-10, 2016*, 2016.
 - [54] M. Misiak et al. Updated NNLO QCD predictions for the weak radiative B-meson decays. *Phys. Rev. Lett.*, 114(22):221801, 2015.
 - [55] Mikolaj Misiak and Matthias Steinhauser. Weak radiative decays of the B meson and bounds on M_{H^\pm} in the Two-Higgs-Doublet Model. *Eur. Phys. J.*, C77(3):201, 2017.
 - [56] A. Arbey, F. Mahmoudi, O. Stal, and T. Stefaniak. Status of the Charged Higgs Boson in Two Higgs Doublet Models. *Eur. Phys. J.*, C78(3):182, 2018.
 - [57] Pere Arnan, Damir Bečirević, Federico Mescia, and Olcyr Sumensari. Two Higgs doublet models and $b \rightarrow s$ exclusive decays. *Eur. Phys. J.*, C77(11):796, 2017.
 - [58] Vardan Khachatryan et al. Search for a charged Higgs boson in pp collisions at $\sqrt{s} = 8$ TeV. *JHEP*, 11:018, 2015.
 - [59] Georges Aad et al. Search for charged Higgs bosons in the $H^\pm \rightarrow tb$ decay channel in pp collisions at $\sqrt{s} = 8$ TeV using the ATLAS detector. *JHEP*, 03:127, 2016.
 - [60] Morad Aaboud et al. Search for charged Higgs bosons produced in association with a top quark and decaying via $H^\pm \rightarrow \tau\nu$ using pp collision data recorded at $\sqrt{s} = 13$ TeV by the ATLAS detector. *Phys. Lett.*, B759:555–574, 2016.
 - [61] Hong-Jian He, Nir Polonsky, and Shu-fang Su. Extra families, Higgs spectrum and oblique corrections. *Phys. Rev.*, D64:053004, 2001.
 - [62] W. Grimus, L. Lavoura, O. M. Ogreid, and P. Osland. The Oblique parameters in multi-Higgs-doublet models. *Nucl. Phys.*, B801:81–96, 2008.
 - [63] Howard E. Haber and Deva O’Neil. Basis-independent methods for the two-Higgs-doublet model III: The CP-conserving limit, custodial symmetry, and the oblique parameters S, T, U. *Phys. Rev.*, D83:055017, 2011.
 - [64] M. Baak, J. Cúth, J. Haller, A. Hoecker, R. Kogler, K. Mönig, M. Schott, and J. Stelzer. The global electroweak fit at NNLO and prospects for the LHC and ILC. *Eur. Phys. J.*, C74:3046, 2014.
 - [65] Abdesslam Arhrib. Unitarity constraints on scalar parameters of the standard and two Higgs doublets model. In *Workshop on Noncommutative Geometry, Superstrings and Particle Physics Rabat, Morocco, June 16-17, 2000*, 2000.

- [66] Shinya Kanemura and Kei Yagyu. Unitarity bound in the most general two Higgs doublet model. *Phys. Lett.*, B751:289–296, 2015.
- [67] A. Barroso, P. M. Ferreira, I. P. Ivanov, and Rui Santos. Metastability bounds on the two Higgs doublet model. *JHEP*, 06:045, 2013.
- [68] Xun-Jie Xu. Tree-level vacuum stability of two-Higgs-doublet models and new constraints on the scalar potential. *Phys. Rev.*, D95(11):115019, 2017.
- [69] Florian Staub. Reopen parameter regions in Two-Higgs Doublet Models. *Phys. Lett.*, B776:407–411, 2018.
- [70] Morad Aaboud et al. Search for heavy resonances decaying into a W or Z boson and a Higgs boson in final states with leptons and b -jets in 36 fb^{-1} of $\sqrt{s} = 13 \text{ TeV}$ pp collisions with the ATLAS detector. 2017.
- [71] Georges Aad et al. Search for a CP-odd Higgs boson decaying to Zh in pp collisions at $\sqrt{s} = 8 \text{ TeV}$ with the ATLAS detector. *Phys. Lett.*, B744:163–183, 2015.
- [72] Vardan Khachatryan et al. Search for a pseudoscalar boson decaying into a Z boson and the 125 GeV Higgs boson in $\ell^+ \ell^- b \bar{b}$ final states. *Phys. Lett.*, B748:221–243, 2015.
- [73] Robert V. Harlander, Stefan Liebler, and Hendrik Mantler. SusHi: A program for the calculation of Higgs production in gluon fusion and bottom-quark annihilation in the Standard Model and the MSSM. *Comput. Phys. Commun.*, 184:1605–1617, 2013.
- [74] T. Plehn, M. Spira, and P. M. Zerwas. Pair production of neutral Higgs particles in gluon-gluon collisions. *Nucl. Phys.*, B479:46–64, 1996. [Erratum: Nucl. Phys.B531,655(1998)].
- [75] T. Hahn and M. Perez-Victoria. Automatized one loop calculations in four-dimensions and D-dimensions. *Comput. Phys. Commun.*, 118:153–165, 1999.
- [76] A. D. Martin, W. J. Stirling, R. S. Thorne, and G. Watt. Parton distributions for the LHC. *Eur. Phys. J.*, C63:189–285, 2009.
- [77] S. Dawson, S. Dittmaier, and M. Spira. Neutral Higgs boson pair production at hadron colliders: QCD corrections. *Phys. Rev.*, D58:115012, 1998.
- [78] Ding Yu Shao, Chong Sheng Li, Hai Tao Li, and Jian Wang. Threshold resummation effects in Higgs boson pair production at the LHC. *JHEP*, 07:169, 2013.
- [79] Daniel de Florian and Javier Mazzitelli. Two-loop virtual corrections to Higgs pair production. *Phys. Lett.*, B724:306–309, 2013.
- [80] Daniel de Florian and Javier Mazzitelli. Higgs Boson Pair Production at Next-to-Next-to-Leading Order in QCD. *Phys. Rev. Lett.*, 111:201801, 2013.
- [81] S. Borowka, N. Greiner, G. Heinrich, S. P. Jones, M. Kerner, J. Schlenk, U. Schubert, and T. Zirke. Higgs Boson Pair Production in Gluon Fusion at Next-to-Leading Order with Full Top-Quark Mass Dependence. *Phys. Rev. Lett.*, 117(1):012001, 2016. [Erratum: Phys. Rev. Lett.117,no.7,079901(2016)].

- [82] Vernon Barger, Lisa L. Everett, C. B. Jackson, Andrea D. Peterson, and Gabe Shaughnessy. New physics in resonant production of Higgs boson pairs. *Phys. Rev. Lett.*, 114(1):011801, 2015.
- [83] Luca Cadamuro. Search and prospects for HH production, 2017, https://indico.in2p3.fr/event/13763/contributions/15195/attachments/12696/15588/5_LucaCadamuro.pdf. https://indico.in2p3.fr/event/13763/contributions/15195/attachments/12696/15588/5_LucaCadamuro.pdf.
- [84] Xiao-Fang Han, Lei Wang, and Jin Min Yang. Higgs pair signal enhanced in the 2HDM with two degenerate 125 GeV Higgs bosons. *Mod. Phys. Lett.*, A31(31):1650178, 2016.
- [85] CEPC-SPPC Study Group. CEPC-SPPC Preliminary Conceptual Design Report. 1. Physics and Detector. 2015.
- [86] Keisuke Fujii et al. Physics Case for the International Linear Collider. 2015.
- [87] M. Bicer et al. First Look at the Physics Case of TLEP. *JHEP*, 01:164, 2014.
- [88] Jiayin Gu, Honglei Li, Zhen Liu, Shufang Su, and Wei Su. Learning from Higgs Physics at Future Higgs Factories. *JHEP*, 12:153, 2017.
- [89] Matthew McCullough. An Indirect Model-Dependent Probe of the Higgs Self-Coupling. *Phys. Rev.*, D90(1):015001, 2014. [Erratum: *Phys. Rev.*D92,no.3,039903(2015)].
- [90] Ties Behnke, James E. Brau, Brian Foster, Juan Fuster, Mike Harrison, James McEwan Paterson, Michael Peskin, Marcel Stanitzki, Nicholas Walker, and Hitoshi Yamamoto. The International Linear Collider Technical Design Report - Volume 1: Executive Summary. 2013.
- [91] Howard Baer, Tim Barklow, Keisuke Fujii, Yuanning Gao, Andre Hoang, Shinya Kanemura, Jenny List, Heather E. Logan, Andrei Nomerotski, Maxim Perelstein, et al. The International Linear Collider Technical Design Report - Volume 2: Physics. 2013.
- [92] Halina Abramowicz et al. The International Linear Collider Technical Design Report - Volume 4: Detectors. 2013.
- [93] Qing-Feng Sun, Feng Feng, Yu Jia, and Wen-Long Sang. Mixed electroweak-QCD corrections to $e^+e^- \rightarrow HZ$ at Higgs factories. *Phys. Rev.*, D96(5):051301, 2017.
- [94] Yinqiang Gong, Zhao Li, Xiaofeng Xu, Li Lin Yang, and Xiaoran Zhao. Mixed QCD-EW corrections for Higgs boson production at e^+e^- colliders. *Phys. Rev.*, D95(9):093003, 2017.
- [95] J. Fleischer and F. Jegerlehner. Radiative Corrections to Higgs Production by $e^+e^- \rightarrow ZH$ in the Weinberg-Salam Model. *Nucl. Phys.*, B216:469–492, 1983.
- [96] Bernd A. Kniehl. Radiative corrections for associated ZH production at future e^+e^- colliders. *Z. Phys.*, C55:605–618, 1992.
- [97] Ansgar Denner, J. Kublbeck, R. Mertig, and M. Bohm. Electroweak radiative corrections to $e^+e^- \rightarrow HZ$. *Z. Phys.*, C56:261–272, 1992.
- [98] Ken-ichi Hikasa. Transverse Polarization Effects in e^+e^- Collisions: The Role of Chiral Symmetry. *Phys. Rev.*, D33:3203, 1986.

- [99] T. Barklow, J. Brau, K. Fujii, J. Gao, J. List, N. Walker, and K. Yokoya. ILC Operating Scenarios. 2015.
- [100] Claude Fabienne Dürig. *Measuring the Higgs Self-coupling at the International Linear Collider*. PhD thesis, Hamburg U., Hamburg, 2016.
- [101] Masakazu Kurata and Tomohiko Tanabe. The Higgs Self Coupling Analysis Using the Events Containing $H \rightarrow WW^*$ Decay. Technical Report LC-REP-2013-025, 2013.